Pergamon

J. Mech. Phys. Solids, Vol. 44, No. 9, pp. 1475–1508, 1996

0022–5096/96 $15.00 + 0.00

PII S0022–5096(96)00037–3

EFFECTS OF ANISOTROPIC HARDENING ON CRACK PROPAGATION IN POROUS-DUCTILE MATERIALS

E. RADI† and D. BIGONI‡

†Istituto di Ingegneria, University of Ferrara, Via Saragat, 1, 44100 Ferrara, Italy

‡Istituto di Scienza delle Costruzioni, University of Bologna, Viale Risorgimento, 2, 40136 Bologna, Italy

(*Received* 10 *August* 1995; *in revised form* 9 *February* 1996)

ABSTRACT

Slow, stable, rectilinear crack propagation is investigated for porous, elastoplastic solids displaying combined isotropic and kinematic hardening. The Gurson model with constant porosity, and therefore the associated flow rule, is used as the constitutive description. An asymptotic analysis of crack-tip fields is performed under Mode I, steady-state, small-strain, plane stress and plane strain conditions. A continuous distribution of asymptotic near-tip fields is found. However, the possibility of the appearance of stress jumps in the asymptotic fields is analysed in detail. The results show many interesting features, which are related to the presence of both porosity and Bauschinger effect. Copyright © 1996 Elsevier Science Ltd

NOTATION

We refer to the abstract tensor notation introduced by Gurtin (1981). Vectors and second order tensors are denoted by bold letters. Lin denotes the set of all tensors and Sym the subset of all symmetric tensors. The natural inner product of tensors is denoted (for any second order tensor $\mathbf{S}$ and $\mathbf{T}$) by $\mathbf{S}\cdot\mathbf{T} = \mathrm{tr}(\mathbf{S}^{\mathrm{T}}\mathbf{T}) = S_{ij}T_{ij}$, where the last equality refers to the introduction of an arbitrary coordinate frame, tr is the trace operator and $(\,)^{\mathrm{T}}$ denotes the transpose of a tensor. The tensor product $\mathbf{a}\otimes\mathbf{b}$ of two vectors $\mathbf{a}$ and $\mathbf{b}$ is the tensor that assigns to each vector $\mathbf{v}$ the vector $(\mathbf{b}\cdot\mathbf{v})\mathbf{a}$. In components: $(\mathbf{a}\otimes\mathbf{b})_{ij} = a_i b_j$.

1. INTRODUCTION

In ductile metals slow, stable crack propagation is often observed before rupture. In particular, for porous metals, porosity may cause a stabilizing effect on crack growth. However, due to the fact that the stress and strain fields in the plastic zone near the tip of a growing crack are subject to strongly non-proportional loading, the conventional theory of incremental plasticity, based on isotropic hardening rules, may overestimate the deformation response in that zone, and hence the capacity of sustaining stable crack growth. Therefore, the influence of anisotropy of strain hardening, i.e. of the Bauschinger effect, which may be relevant to crack propagation in ductile-porous solids, is the focus of this paper.

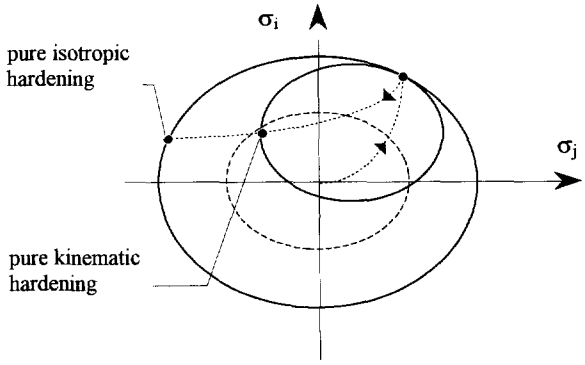

Fig. 1. Schematic representation of isotropic and kinematic hardening behaviors for non-proportional loading.

The first asymptotic analysis of steady-state crack propagation in a linear isotropic hardening J_2-flow theory material was given by Amazigo and Hutchinson (1977) and later generalized in different ways (Achenbach *et al.*, 1981; Ponte Castañeda, 1987; Östlund and Gudmundson, 1988; Bigoni and Radi, 1993; Radi and Bigoni, 1993, 1994). Zhang *et al.* (1983, 1984) obtained the only asymptotic analysis available in the literature concerning Mode I propagation for a mixed isotropic–kinematic hardening J_2-flow theory material. Their analysis has been recently completed by Bigoni and Radi (1996), where Mode III propagation has been solved. Porous elastoplastic metals were considered recently for the cases of stationary and growing cracks for perfectly plastic behavior (Drugan and Miao, 1992; Miao and Drugan, 1993, 1995) and for isotropic hardening (Radi and Bigoni, 1994), all employing a constant porosity version of the Gurson model (Gurson, 1977a, b). The Gurson model, which may describe the behavior of porous metals and particulate-reinforced metal matrix composites, was generalized by Mear and Hutchinson (1985) through the introduction of mixed isotropic–kinematic hardening. The Mear and Hutchinson version of the Gurson model has been employed to show that for non-proportional stress histories, the J_2-flow theory tends to be overly stiff when used to predict plastic instabilities (Tvergaard, 1978, 1987; Becker and Needleman, 1986; Tvergaard and van der Giessen, 1991). When isotropic hardening is used in the analysis of near crack-tip fields, the elastic domain of a material particle in the proximity of the crack tip greatly increases, due to the severe plastic deformations caused by the stress singularity. Therefore, isotropic hardening produces a lower level of plastic deformation than would be produced for kinematic hardening (Fig. 1).

In addition to the asymptotic solutions given by Zhang *et al.* (1983) and Bigoni and Radi (1996), there are a number of finite element simulations of crack growth in elastoplastic homogeneous material with anisotropic hardening, within the framework of J_2-flow theory (Lam and McMeeking, 1984; Narasimhan and Venkatesha, 1993; Narasimhan *et al.*, 1993), and in the case of the Gurson model (Aoki *et al.*, 1987; Jagota *et al.*, 1987; Needleman and Tvergaard, 1987; Tvergaard and Needleman, 1992). Several results obtained in these works are qualitatively confirmed in the present paper. In particular, Lam and McMeeking (1984) investigated the influence

of corner formation on the yield surface, and of the Bauschinger effect. A large reduction was found in the magnitude of stress components due to kinematic hardening, together with a continuing decrease of the flow stress after the passage of the crack tip. Narasimhan and Venkatesha (1993) simulated steady-state dynamic crack propagation under Mode I plane strain conditions, in materials displaying isotropic and anisotropic hardening. One of their conclusions is that for kinematic hardening, no elastic unloading occurs for low crack speed. Narasimhan *et al.* (1993) extended this analysis to plane stress condition showing that the main difference between the near-tip stress fields for isotropic and kinematic hardening is in the region behind the crack tip, where a thick secondary plastic reloading sector is found in the case of kinematic hardening only.

A generalization of the procedure introduced by Ponte Castañeda (1987) is employed in this paper to obtain an asymptotic analysis of steady-state crack propagation in an elastoplastic material obeying the mixed kinematic–isotropic hardening Gurson model (Mear and Hutchinson, 1985; see also Tvergaard, 1987). Reference is made to the incremental theory of plasticity, which makes it possible to consider elastic unloading and subsequent plastic reloading in the crack wake. The analysis is carried out under the hypothesis of uniform porosity, which may be valid for modeling the behavior of incompletely sintered, or previously deformed metals, or materials fabricated with intentional initial porosity (such as, e.g., HIPed porous materials, see Ishizaki and Nanko, 1995). Beside the applicability to these materials, it should be noted that the assumption of constant porosity may be reasonable in the range of validity of the asymptotic analysis, since the results obtained from this kind of analysis are valid outside of the very near crack-tip zone, where micro-inhomogeneities, cavitation and finite deformation effects dominate. As noted by Drugan and Miao (1992), large deformation numerical finite element solutions employing the Gurson model show that outside the usual large-strain near-tip region, porosity changes are negligible. In any case, when a nucleation law for the porosity is included, the crack-tip fields may not admit a separate-variable form and their determination may require finite element investigations. On the other hand, it is precisely in the zone where the assumption of constant porosity is reasonable that the linear kinematic-hardening model is meaningful. At large deformations, in fact, there seems to be no experimental indication of significant Bauschinger effect, whereas its significance at small strains is certain. In conclusion, it is precisely in the range of applicability of the asymptotic analysis that the assumptions of constant porosity, linear kinematic hardening, and small strains are correct, and therefore the analysis carried out in this paper can be considered on the one hand mathematically consistent, and, on the other hand, based on a proper material model.

Results are given in this article for the near-tip stress and velocity fields as functions of porosity and mixed hardening parameter. Both plane strain and plane stress Mode I crack propagation are analyzed. Many previous results are obtained as special cases of the present formulation. In particular, results obtained in the limit case of pure isotropic hardening coincide with those obtained by Radi and Bigoni (1994), and, when the porosity becomes zero, the J_2-flow theory is recovered, and results reduce to those by Ponte Castañeda (1987) for isotropic hardening, and to those of Zhang *et al.* (1983, 1984) for mixed hardening. In this last particular case, results will be given

which complete those by Zhang *et al.* (1983, 1984), presenting a wider exploration of material parameters. These authors in fact apparently did not note that the asymptotic stress fields exhibit rapid variations, for a sufficiently high component of kinematic hardening, a circumstance analysed in detail in this paper.

The analysis presented elucidates the effects of porosity and of anisotropic hardening on the local crack-tip fields. In particular, since a material point close to the crack-tip trajectory is subject to one cycle of loading, the Bauschinger effect results in a strong influence on the stress fields. Due to the presence of a larger reloading sector adjacent to the crack flank, this effect is more pronounced under plane strain, as opposed to plane stress, loading conditions.

Finally, it is worth mentioning that the obtained asymptotic fields always correspond to continuous stress and velocity distributions. This is consistent with a theorem by Drugan and Rice (1984), whose constitutive range of validity was recently extended by Drugan (1995). All constitutive response modeled here is included in this extended theorem. The "transition" value of the mixity hardening parameter is obtained in the present paper for the case when the current yield locus does not incorporate all prior yield loci [condition corresponding to the violation of Drugan and Rice (1984) jump exclusion condition]. Although Drugan's (1995) new result is valid beyond this limit, and our solution does remain fully continuous beyond it, it is interesting to note that, when the mixity parameter goes beyond this value, the obtained solutions display a rapid variation in the fields.

2. CONSTITUTIVE EQUATIONS

Reference is made to the Gurson model of elastoplastic solids containing spherical voids. The model is based on a family of isotropic–kinematic hardening yield surfaces of the form $\varphi(\boldsymbol{\sigma}, \boldsymbol{\alpha}, \sigma_F, \phi) = 0$, where ϕ is the volume fraction of voids, $\boldsymbol{\sigma}$ is the average macroscopic stress tensor and $\boldsymbol{\alpha}$ denotes the back stress tensor. The variable σ_F is related to the behavior of the matrix material. In particular, when the matrix material is modeled through the J_2-flow theory, the internal variable σ_F equals the radius of the current yield surface of the matrix, and is therefore given by

$$\sigma_F = (1-b)\sigma_0 + b\sigma_m, \tag{2.1}$$

where σ_0 and σ_m are the initial yield stress and the current flow stress of the matrix, respectively. Constant b is a mixed hardening parameter, which ranges between 0, for pure kinematic hardening, and 1, for pure isotropic hardening.

The Gurson yield condition for a porous solid is taken in the form proposed by Mear and Hutchinson (1985)

$$f(\boldsymbol{\sigma}, \boldsymbol{\alpha}, \sigma_F) = \frac{3|\operatorname{dev}\tilde{\boldsymbol{\sigma}}|^2}{2\sigma_F^2} + 2\phi\cosh\left(\frac{\operatorname{tr}\tilde{\boldsymbol{\sigma}}}{2\sigma_F}\right) - (1+\phi^2) = 0, \tag{2.2}$$

where $\tilde{\boldsymbol{\sigma}} = \boldsymbol{\sigma} - \boldsymbol{\alpha}$, and $\operatorname{dev}\tilde{\boldsymbol{\sigma}}$ denotes the deviatoric part of $\tilde{\boldsymbol{\sigma}}$. The generalization of the yield function proposed by Tvergaard (1981, 1982, 1987) and Tvergaard and van der Giessen (1991), which could be easily included, is not considered for the sake of

simplicity. Moreover, the void volume fraction ϕ is assumed constant [the same hypothesis was made also in Drugan and Miao (1992), Miao and Drugan (1993, 1995) and Radi and Bigoni (1994)]; therefore ϕ is not an internal variable subject to evolution. Since nucleation and growth of voids has been neglected, the condition of associativity for the matrix material implies an associated plastic flow law for the macroscopic porous material, i.e.

$$\dot{\boldsymbol{\varepsilon}}^{\mathrm{P}} = \Lambda \mathbf{Q}, \tag{2.3}$$

where Λ is the (non-negative) plastic multiplier and $\mathbf{Q}$ is proportional to the gradient of the yield function (2.2), namely

$$\mathbf{Q} = \frac{\sigma_{\mathrm{F}}}{2}\frac{\partial f}{\partial \boldsymbol{\sigma}} = \frac{3}{2\sigma_{\mathrm{F}}}\operatorname{dev}\tilde{\boldsymbol{\sigma}} + \gamma \mathbf{I}, \quad \gamma = \frac{\phi}{2}\sinh\left(\frac{\operatorname{tr}\tilde{\boldsymbol{\sigma}}}{2\sigma_{\mathrm{F}}}\right). \tag{2.4}$$

The evolution law for the back stress is assumed in agreement with the Ziegler (1959) hardening rule, in the form

$$\dot{\boldsymbol{\alpha}} = \mu \Lambda \tilde{\boldsymbol{\sigma}}, \tag{2.5}$$

where μ specifies the modulus of $\dot{\boldsymbol{\alpha}}$.

As in Tvergaard (1987), the macroscopic plastic strain rate $\dot{\boldsymbol{\varepsilon}}^{\mathrm{P}}$ is assumed to be related to the effective plastic strain rate $\dot{\varepsilon}_{\mathrm{m}}^{\mathrm{P}}$ of the matrix material, by

$$\tilde{\boldsymbol{\sigma}} \cdot \dot{\boldsymbol{\varepsilon}}^{\mathrm{P}} = (1-\phi)\sigma_{\mathrm{F}}\dot{\varepsilon}_{\mathrm{m}}^{\mathrm{P}}. \tag{2.6}$$

Note that, for $b = 1$, (2.6) reduces to the equivalent plastic work relationship adopted by Gurson (1977a). When the mechanical behavior of the metallic matrix is modeled through an elastoplastic constitutive law displaying linear hardening, the equivalent stress rate is related to the effective plastic strain rate by the following linear relation, derived from the uniaxial stress–strain bilinear relation of the matrix material

$$\dot{\sigma}_{\mathrm{m}} = 3H_{\mathrm{m}}\dot{\varepsilon}_{\mathrm{m}}^{\mathrm{P}}, \tag{2.7}$$

where H_{m} is the hardening modulus of the matrix material, which depends on the ratio $\alpha_{\mathrm{G}} = G_{\mathrm{t}}/G$ of the current tangential modulus to the elastic shear modulus of the matrix material, or on the ratio $\alpha_{\mathrm{E}} = E_{\mathrm{t}}/E$ of current tensile modulus to the elastic Young's modulus

$$H_{\mathrm{m}} = \frac{\alpha_{\mathrm{G}}}{1-\alpha_{\mathrm{G}}}G, \quad H_{\mathrm{m}} = \frac{\alpha_{\mathrm{E}}}{3(1-\alpha_{\mathrm{E}})}E. \tag{2.8}$$

The evolution law for σ_{F} may be derived from (2.1) written in incremental form, i.e. $\dot{\sigma}_{\mathrm{F}} = b\dot{\sigma}_{\mathrm{m}}$, using (2.3), (2.6) and (2.7)

$$\dot{\sigma}_{\mathrm{F}} = \Lambda \frac{3H_{\mathrm{m}}b}{(1-\phi)\sigma_{\mathrm{F}}}\mathbf{Q} \cdot \tilde{\boldsymbol{\sigma}}. \tag{2.9}$$

Prager consistency must be satisfied during plastic flow, whence the expression of the plastic multiplier may be derived

$$\Lambda = \frac{\langle \mathbf{Q} \cdot \dot{\boldsymbol{\sigma}} \rangle}{H}, \tag{2.10}$$

where $\langle\ \rangle$, the Macaulay brackets, implies the value of the argument when it is positive but zero otherwise, and

$$H = (\mathbf{Q} \cdot \tilde{\boldsymbol{\sigma}}) \left[\mu + \frac{3H_{\mathrm{m}} b}{(1-\phi)\sigma_{\mathrm{F}}^2} \mathbf{Q} \cdot \tilde{\boldsymbol{\sigma}} \right] \tag{2.11}$$

is the macroscopic hardening modulus of the porous material.

The elastoplastic model is completely determined when function μ is specified. However, there is some freedom in determining this function. Following Mear and Hutchinson (1985) and Tvergaard (1987), we require that the mixed isotropic–kinematic hardening model and the isotropic hardening Gurson model give identical response for proportional stress histories. In the following, index $(\,)_{\mathrm{G}}$ denotes quantities referring to the Gurson isotropic hardening model, which is characterized by the yield function $f_{\mathrm{G}} = f(\boldsymbol{\sigma}_{\mathrm{G}}, \sigma_{\mathrm{m}}, \phi)$. For proportional stress histories, let $\tilde{\boldsymbol{\sigma}} = \gamma \boldsymbol{\xi}$ and $\boldsymbol{\sigma}_{\mathrm{G}} = \gamma_{\mathrm{G}} \boldsymbol{\xi}$, where the (unit norm) second order tensor $\boldsymbol{\xi}$ specifies the direction of the radial path in stress space and γ and γ_{G} the moduli. By assumption, $\tilde{\boldsymbol{\sigma}}$ satisfies (2.2), and when

$$\frac{\gamma_{\mathrm{G}}}{\gamma} = \frac{\sigma_{\mathrm{m}}}{\sigma_{\mathrm{F}}}, \tag{2.12}$$

$\boldsymbol{\sigma}_{\mathrm{G}}$ also satisfies $f(\boldsymbol{\sigma}_{\mathrm{G}}, \sigma_{\mathrm{m}}, \phi) = 0$. Note that condition (2.12) implies $\mathbf{Q}_{\mathrm{G}} = \mathbf{Q}$. Therefore, for a fixed stress rate $\dot{\boldsymbol{\sigma}}$, the mixed kinematic hardening and the isotropic models give the same plastic strain rate $\dot{\boldsymbol{\varepsilon}}^{\mathrm{p}}$ when the plastic multiplier is the same for both models, i.e. when $\Lambda = \Lambda_{\mathrm{G}}$. This condition implies that H must be equal to the hardening modulus H_{G} of the Gurson isotropic model [see, e.g., Radi and Bigoni (1994)]; therefore

$$\frac{3H_{\mathrm{m}}}{(1-\phi)\sigma_{\mathrm{m}}^2} [\mathbf{Q} \cdot (\gamma_{\mathrm{G}} \boldsymbol{\xi})]^2 = \left[\mu + \frac{3H_{\mathrm{m}} b}{(1-\phi)\sigma_{\mathrm{F}}^2} \mathbf{Q} \cdot (\gamma \boldsymbol{\xi}) \right] \mathbf{Q} \cdot (\gamma \boldsymbol{\xi}). \tag{2.13}$$

By introducing condition (2.12) into (2.13) and generalizing to any stress state, namely, by replacing $\gamma \boldsymbol{\xi}$ by $\tilde{\boldsymbol{\sigma}}$, μ can be obtained

$$\mu = (1-b) \frac{3H_{\mathrm{m}}}{(1-\phi)\sigma_{\mathrm{F}}^2} \mathbf{Q} \cdot \tilde{\boldsymbol{\sigma}}. \tag{2.14}$$

When expression (2.14) of μ is employed, the macroscopic hardening modulus (2.11) becomes

$$H = \frac{3H_{\mathrm{m}}}{(1-\phi)\sigma_{\mathrm{F}}^2} (\mathbf{Q} \cdot \tilde{\boldsymbol{\sigma}})^2. \tag{2.15}$$

Note from (2.7) that a positive hardening modulus of the matrix material H_{m} results in a positive hardening modulus H of the porous material. In the following, the

dimensionless hardening moduli of the metallic matrix and of the macroscopic porous material are denoted by $h_m = H_m/E$ and $h = H/E$, respectively.

The rate of translation and growth of the yield surface, measured by $\dot{\boldsymbol{\alpha}}$ and $\dot{\sigma}_F$, becomes fully specified when the expression (2.10) for the plastic multiplier Λ is introduced into (2.9) and (2.5)

$$\dot{\boldsymbol{\alpha}} = (1-b)\frac{\langle \mathbf{Q}\cdot\dot{\boldsymbol{\sigma}}\rangle}{\mathbf{Q}\cdot\tilde{\boldsymbol{\sigma}}}\tilde{\boldsymbol{\sigma}}, \quad \dot{\sigma}_F = b\frac{\langle \mathbf{Q}\cdot\dot{\boldsymbol{\sigma}}\rangle}{\mathbf{Q}\cdot\tilde{\boldsymbol{\sigma}}}\sigma_F. \tag{2.16}$$

If the elastic behavior is assumed isotropic, the elastoplastic incremental constitutive equations relating the stress rate $\dot{\boldsymbol{\sigma}}$ to the velocity of deformation $\dot{\boldsymbol{\varepsilon}}$, can finally be written in the standard form

$$\dot{\boldsymbol{\varepsilon}} = \frac{1}{2G}\left[\dot{\boldsymbol{\sigma}} - \frac{\nu}{1+\nu}(\operatorname{tr}\dot{\boldsymbol{\sigma}})\mathbf{I}\right] + \Lambda\mathbf{Q}, \tag{2.17}$$

where ν is the Poisson ratio. Equations (2.16) and (2.17) hold when the stress state satisfies the yield condition (2.2). Otherwise, the incremental constitutive relationship reduces to the elastic isotropic behavior, which can formally be obtained from (2.17) by setting $\Lambda = 0$.

3. CRACK PROPAGATION

3.1. *Problem formulation*

The problem of a plane crack quasi-statically propagating at constant velocity c, along a rectilinear path in an infinite medium, is considered. The mechanical behavior of the material is described by the anisotropic-hardening, incremental elastoplastic constitutive law presented in Section 2. This framework allows incorporation of elastic unloading sectors, which may appear in the proximity of the crack tip during crack propagation. A cylindrical coordinate system $(O, \mathbf{e}_r, \mathbf{e}_\vartheta, \mathbf{e}_3)$ moving with the crack tip in the $\vartheta = 0$ direction is adopted, with the x_3-axis along the straight crack front. The steady-state condition yields the following time derivative rule, for any scalar, vector or second order tensor $\mathbf{X}$

$$\dot{\mathbf{X}} = \frac{c}{r}\left[\frac{\partial \mathbf{X}}{\partial \vartheta}\sin\vartheta - r\frac{\partial \mathbf{X}}{\partial r}\cos\vartheta\right], \tag{3.1}$$

where r and ϑ are the polar coordinates in the plane orthogonal to the x_3-axis. It is important to remark that the components of the derivatives of a tensor $\mathbf{X}$ are different from the derivatives of the components. In the following, the derivatives of a tensor $\mathbf{X}$ and of its components with respect to ϑ are denoted by $\mathbf{X}'$, and by $X_{\alpha\beta,\vartheta}$, respectively.

The kinematic compatibility condition between strain rates and velocities is

$$\dot{\boldsymbol{\varepsilon}} = \tfrac{1}{2}(\nabla\mathbf{v} + \nabla\mathbf{v}^T). \tag{3.2}$$

The condition $\dot{\varepsilon}_{33} = 0$ must be considered in addition to (3.2), for the plane strain problem.

The quasistatic equilibrium condition is

$$\operatorname{div}\boldsymbol{\sigma} = \mathbf{0}. \tag{3.3}$$

Compatibility (3.2), equilibrium (3.3) and the incremental constitutive equations (2.16) and (2.17) form a system of first order PDEs which governs the problem of crack propagation. The solution is sought in a separable-variable form, by considering single-term asymptotic expansions of near crack-tip fields. In particular, the stress, back stress, velocity, and flow stress fields are assumed in the forms

$$\mathbf{v}(r,\vartheta) = \frac{c}{s}\left(\frac{r}{B}\right)^s \mathbf{w}(\vartheta), \quad \boldsymbol{\sigma}(r,\vartheta) = E\left(\frac{r}{B}\right)^s \mathbf{T}(\vartheta),$$

$$\boldsymbol{\alpha}(r,\vartheta) = E\left(\frac{r}{B}\right)^s \mathbf{A}(\vartheta), \quad \sigma_{\mathrm{F}}(r,\vartheta) = E\left(\frac{r}{B}\right)^s T_{\mathrm{F}}(\vartheta), \tag{3.4}$$

where s is the exponent of the fields singularity and B denotes a characteristic dimension of the plastic zone. Observe that s and functions $\mathbf{w}$, $\mathbf{T}$, $\mathbf{A}$ and T_{F} are the unknowns of the problem and do not depend on the value of the crack propagation velocity c, since inertia is not accounted for. Moreover, the characteristic dimension B of the plastic zone remains undetermined, since the asymptotic problem is homogeneous. For finite geometry of the body containing the crack, the determination of the amplitude of the asymptotic fields requires a matching procedure with the applicable boundary conditions.

The material time rates of the fields $\boldsymbol{\sigma}$, $\boldsymbol{\alpha}$ and σ_{F} may be derived from representation (3.4) by using the steady-state derivative (3.1) in the form

$$\dot{\boldsymbol{\sigma}}(r,\vartheta) = E\frac{c}{r}\left(\frac{r}{B}\right)^s \boldsymbol{\Sigma}(\vartheta),$$

$$\dot{\boldsymbol{\alpha}}(r,\vartheta) = E\frac{c}{r}\left(\frac{r}{B}\right)^s \boldsymbol{\Omega}(\vartheta),$$

$$\dot{\sigma}_{\mathrm{F}}(r,\vartheta) = E\frac{c}{r}\left(\frac{r}{B}\right)^s \Sigma_{\mathrm{F}}(\vartheta), \tag{3.5}$$

where the functions $\boldsymbol{\Sigma}$, $\boldsymbol{\Omega}$ and Σ_{F}, which are independent of r, may be written, using representation (3.4), in the form

$$\boldsymbol{\Sigma} = \mathbf{T}'\sin\vartheta - s\mathbf{T}\cos\vartheta,$$

$$\boldsymbol{\Omega} = \mathbf{A}'\sin\vartheta - s\mathbf{A}\cos\vartheta,$$

$$\Sigma_{\mathrm{F}} = T'_{\mathrm{F}}\sin\vartheta - sT_{\mathrm{F}}\cos\vartheta. \tag{3.6}$$

When the asymptotic fields (3.4) are introduced into equilibrium equations (3.3), the following ordinary differential equations are derived (see Appendix 1)

$$\mathbf{T}'\mathbf{e}_\vartheta + s\mathbf{T}\mathbf{e}_r = \mathbf{0}. \tag{3.7}$$

Equation (3.7) gives the following two scalar equations

$$T_{r\vartheta,\vartheta} = -(1+s)T_{rr} + T_{\vartheta\vartheta},$$
$$T_{\vartheta\vartheta,\vartheta} = -(2+s)T_{r\vartheta}. \tag{3.8}$$

By applying (3.6_1) to the unit vector $\mathbf{e}_\vartheta$, using equilibrium equations (3.7) and, finally, relations (A1.1), the following condition can be derived

$$\boldsymbol{\Sigma}\mathbf{e}_\vartheta = -s\mathbf{T}(\mathbf{e}_r \sin\vartheta + \mathbf{e}_\vartheta \cos\vartheta) = -s\mathbf{T}\mathbf{e}_2, \tag{3.9}$$

which gives the stress rate components $\Sigma_{r\vartheta}$ and $\Sigma_{\vartheta\vartheta}$ as functions of the components of the stress tensor $\mathbf{T}$.

Finally, the strain rates (3.2), which correspond to the velocity fields (3.4_1), are

$$\dot{\boldsymbol{\varepsilon}} = \frac{c}{sr}\left(\frac{r}{B}\right)^s [\mathbf{w}' \otimes \mathbf{e}_\vartheta + s\mathbf{w} \otimes \mathbf{e}_r]_{\mathrm{Sym}}, \tag{3.10}$$

where symbol $[\,]_{\mathrm{Sym}}$ denotes the symmetric part of the tensor argument.

It is worth noting that, when the asymptotic fields (3.4) are introduced into the yield function (2.2) and its gradient (2.4), these become independent of r. Therefore, $f(\boldsymbol{\sigma}, \boldsymbol{\alpha}, \sigma_F) = f(\mathbf{T}, \mathbf{A}, T_F)$, and the yield condition and yield function gradient become

$$f(\mathbf{T}, \mathbf{A}, T_F) = \frac{3|\mathrm{dev}\,\tilde{\mathbf{T}}|^2}{2T_F^2} + 2\phi\cosh\left(\frac{\mathrm{tr}\,\tilde{\mathbf{T}}}{2T_F}\right) - (1+\phi^2) = 0, \tag{3.11}$$

and

$$\mathbf{Q} = \frac{3}{2T_F}\mathrm{dev}\,\tilde{\mathbf{T}} + \gamma\mathbf{I}, \quad \gamma = \frac{\phi}{2}\sinh\left(\frac{\mathrm{tr}\,\tilde{\mathbf{T}}}{2T_F}\right), \tag{3.12}$$

where $\tilde{\mathbf{T}} = \mathbf{T} - \mathbf{A}$.

As a consequence of relation (3.5_1), the plastic multiplier (2.10) may be written as

$$\Lambda = \frac{c}{r}\left(\frac{r}{B}\right)^s \langle\lambda\rangle, \quad \lambda = \frac{\mathbf{Q}\cdot\boldsymbol{\Sigma}}{h}, \tag{3.13}$$

where h is the dimensionless hardening modulus of the porous material. Noting (3.4), h may be expressed in the form

$$h = \frac{3h_m}{(1-\phi)}\frac{(\mathbf{Q}\cdot\tilde{\mathbf{T}})^2}{T_F^2}. \tag{3.14}$$

It should be observed that h is always greater than zero, since porous metals with positive hardening modulus of the matrix material ($H_m > 0$) are considered (the product $\mathbf{Q}\cdot\tilde{\mathbf{T}}$ vanishes if and only if $\tilde{\mathbf{T}} = \mathbf{0}$, which may occur only when the stress point is inside the yield locus).

When the asymptotic fields (3.4) and their rates (3.5) are introduced into the

incremental constitutive relationships (2.16) and (2.17), a system of nine equations is obtained, namely

$$\left(\frac{1}{s}\mathbf{w}'\otimes\mathbf{e}_\vartheta+\mathbf{w}\otimes\mathbf{e}_r\right)_{\text{Sym}}=(1+\nu)\boldsymbol{\Sigma}-\nu\,\text{tr}\,\boldsymbol{\Sigma}\mathbf{I}+\langle\lambda\rangle\mathbf{Q}, \tag{3.15}$$

$$\mathbf{A}'\sin\vartheta=s\mathbf{A}\cos\vartheta+(1-b)\langle\rho\rangle\tilde{\mathbf{T}}, \tag{3.16}$$

$$T_F'\sin\vartheta=sT_F\cos\vartheta+b\langle\rho\rangle T_F, \tag{3.17}$$

where

$$\rho=\frac{\mathbf{Q}\cdot\boldsymbol{\Sigma}}{\mathbf{Q}\cdot\tilde{\mathbf{T}}}. \tag{3.18}$$

The constitutive equations (3.15)–(3.17) are valid when the stress point lies on the yield surface. During elastic unloading or neutral loading, the constitutive relation (3.15) reduces to the incremental equation of linear isotropic elasticity, and (3.16) and (3.17) become equivalent to the conditions $\dot{\boldsymbol{\alpha}}=\mathbf{0}$ and $\dot{\sigma}_F=0$.

System (3.15)–(3.17), together with the equilibrium equations (3.7), results in 11 first order ODEs of homogeneous type, for the 11 unknown components of the angular functions $\mathbf{w}$, $\mathbf{T}$, $\mathbf{A}$ and T_F. The components of these functions reduce to nine under plane stress, where T_{33} and A_{33} vanish. The unknown exponent s may be determined as an eigenvalue of the problem, when a normalization condition for the solution is considered. A lucid discussion on the formulation of a crack propagation problem in terms of a generalized non-linear eigenvalue problem has been given by Bose and Ponte Castañeda (1992).

The ODEs (3.16) and (3.17) are in explicit form $[y'(\vartheta)=f(y(\vartheta),\vartheta)]$, whereas (3.15) is still in implicit form. In order to obtain the explicit forms, some algebraic manipulations are necessary. In particular, by considering the components rr and 33 of the constitutive equations (3.15), and using the plane strain condition, the following system of equations may be derived

$$\begin{aligned}(h+Q_{rr}^2)\Sigma_{rr}-(\nu h-Q_{rr}Q_{33})\Sigma_{33}&=w_r h+(\nu h-Q_{rr}Q_{\vartheta\vartheta})\Sigma_{\vartheta\vartheta}-2Q_{rr}Q_{r\vartheta}\Sigma_{r\vartheta},\\(\nu h-Q_{rr}Q_{33})\Sigma_{rr}-(h+Q_{33}^2)\Sigma_{33}&=2Q_{33}Q_{r\vartheta}\Sigma_{r\vartheta}-(\nu h-Q_{33}Q_{\vartheta\vartheta})\Sigma_{\vartheta\vartheta}.\end{aligned} \tag{3.19}$$

Equations (3.9) make explicit that $\Sigma_{\vartheta\vartheta}$ and $\Sigma_{r\vartheta}$ are independent of the components of $\mathbf{T}'$, and, therefore, the right hand sides of relations (3.19) are independent of these also. Equations (3.19) may be solved for Σ_{rr} and Σ_{33}. In particular, Σ_{rr} can be obtained in the following form

$$\begin{aligned}\Sigma_{rr}=\frac{1}{\Delta}\{&\Sigma_{\vartheta\vartheta}[\nu(1+\nu)h+\nu Q_{33}(Q_{33}-Q_{\vartheta\vartheta})-Q_{rr}(\nu Q_{33}+Q_{\vartheta\vartheta})]\\&-2\Sigma_{r\vartheta}Q_{r\vartheta}(\nu Q_{33}+Q_{rr})+w_r(h+Q_{33}^2)\},\end{aligned} \tag{3.20}$$

where $\Delta=(1-\nu^2)h+Q_{33}^2+Q_{rr}^2+2\nu Q_{rr}Q_{33}$, is always greater than zero. With Σ_{rr} known from (3.20), Σ_{33} may be obtained from a rearrangement of (3.19_2). When Σ_{rr} and Σ_{33} are substituted into (3.6_1), the derivatives with respect to the angular coordinate ϑ of the stress components T_{rr} and T_{33} may be obtained

$$T_{rr,\vartheta} = 2T_{r\vartheta} + (sT_{rr}\cos\vartheta + \Sigma_{rr})/\sin\vartheta,$$
$$T_{33,\vartheta} = (sT_{33}\cos\vartheta + \Sigma_{33})/\sin\vartheta. \tag{3.21}$$

The expressions for $w_{r,\vartheta}$ and $w_{\vartheta,\vartheta}$ follow from the constitutive relations (3.15)

$$w_{r,\vartheta} = (1-s)w_\vartheta + 2s[(1+\nu)\Sigma_{r\vartheta} + \langle\lambda\rangle Q_{r\vartheta}],$$
$$w_{\vartheta,\vartheta} = -w_r + s[\Sigma_{\vartheta\vartheta} - \nu(\Sigma_{rr}+\Sigma_{33}) + \langle\lambda\rangle Q_{\vartheta\vartheta}]. \tag{3.22}$$

Equations (3.8), (3.16), (3.17), (3.21) and (3.22) form the first order ODE system, which governs the near-tip stress and velocity fields. This system may be written in the following form

$$\mathbf{y}'(\vartheta) = \begin{cases} \mathbf{f}_p(\vartheta, \mathbf{y}(\vartheta), s) \text{ if } f(\mathbf{T}, \mathbf{A}, T_F) = 0 \quad \text{and} \quad \mathbf{Q}\cdot\boldsymbol{\Sigma} > 0, \\ \mathbf{f}_e(\vartheta, \mathbf{y}(\vartheta), s) \text{ if } f(\mathbf{T}, \mathbf{A}, T_F) < 0 \text{ or } f(\mathbf{T}, \mathbf{A}, T_F) = 0 \quad \text{and} \quad \mathbf{Q}\cdot\boldsymbol{\Sigma} \leqslant 0, \end{cases} \tag{3.23}$$

where $\mathbf{y} = \{w_r, w_\vartheta, T_{r\vartheta}, T_{rr}, T_{\vartheta\vartheta}, T_{33}, A_{r\vartheta}, A_{rr}, A_{\vartheta\vartheta}, A_{33}, T_F\}$.

3.2. *Elastic unloading and secondary plastic reloading*

The motion of the material particles close to the trajectory of the crack tip is assumed to occur along a straight path, parallel to the crack-tip trajectory (Fig. 2). This assumption, consistent within the framework of the infinitesimal theory, is widely accepted (see, e.g., Ponte Castañeda, 1987). A generic material point near the trajectory of the crack tip experiences, in general, plastic loading, elastic unloading and subsequent plastic reloading. The angular coordinate ϑ singles out the position of a material point moving along its rectilinear path at a fixed distance, say d, from the crack line. The straight path of a generic point is defined by the geometric relation $r(\vartheta) = d/\sin\vartheta$.

A material point, initially ahead of the crack tip, leaves the plastic loading sector when $\mathbf{Q}(\vartheta_1)\cdot\boldsymbol{\Sigma}(\vartheta_1) = 0$, which is the condition determining the elastic unloading angle ϑ_1. In the elastic unloading sector, the plastic multiplier Λ vanishes, and the rate constitutive law (2.17) reduces to the linear isotropic elastic relation. Throughout this sector the back stress $\boldsymbol{\alpha}$ and the flow stress σ_F remain constant for each material point, and equal to their values at the elastic unloading angle ϑ_1, namely

$$\boldsymbol{\alpha}[r(\vartheta), \vartheta] = \boldsymbol{\alpha}[r(\vartheta_1), \vartheta_1], \quad \sigma_F[r(\vartheta), \vartheta] = \sigma_F[r(\vartheta_1), \vartheta_1], \tag{3.24}$$

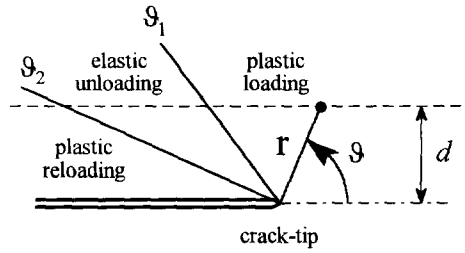

Fig. 2. Crack-tip geometry.

for $\vartheta_1 \leqslant \vartheta \leqslant \vartheta_2$, where ϑ_2 denotes the plastic reloading angle (Fig. 2). The representations ($3.4_{3,4}$) of $\boldsymbol{\alpha}$ and σ_F, and conditions (3.24), imply that functions $\mathbf{A}$ and T_F have the following dependence on the polar coordinate ϑ in the elastic sector

$$\mathbf{A} = \left(\frac{\sin\vartheta}{\sin\vartheta_1}\right)^s \mathbf{A}(\vartheta_1), \quad T_F = \left(\frac{\sin\vartheta}{\sin\vartheta_1}\right)^s T_F(\vartheta_1), \tag{3.25}$$

for $\vartheta_1 \leqslant \vartheta \leqslant \vartheta_2$ [the equivalence of (3.25) to $\dot{\boldsymbol{\alpha}} = \mathbf{0}$ and $\dot{\sigma}_F = 0$ may be appreciated considering ($3.6_{2,3}$)]. Plastic reloading adjacent to the crack flanks occurs when the particle reaches a stress state lying on the yield surface in the form it had developed when unloading began. Thus reloading takes place at the angle ϑ_2, which satisfies

$$f\{\boldsymbol{\sigma}[r(\vartheta_2), \vartheta_2], \boldsymbol{\alpha}[r(\vartheta_1), \vartheta_1], \sigma_F[r(\vartheta_1), \vartheta_1]\} = 0. \tag{3.26}$$

3.3. *Pure kinematic hardening limit*

In the limit case of pure kinematic hardening, i.e. for $b = 0$, the yield surface does not change in dimension, therefore, the parameter σ_F is constant and equal to the yield stress σ_0. Considering the form (2.2) of yield function, it can be concluded that the reduced stress remains finite even when the crack tip is approached, i.e. when $r \to 0$. From this observation, and assuming the separable variable representation (3.4) of stress and back stress fields, the singular terms of these quantities must coincide, namely at first order stress and back stress angular function must be equal: $\mathbf{T} = \mathbf{A}$, and the reduced stress $\tilde{\mathbf{T}}$ can be determined by introducing higher order terms. Therefore, the first order asymptotic representation used in this paper is not sufficient for obtaining the near crack-tip fields, in the limit case of pure kinematic hardening. A higher order field representation is necessary. The results presented in Sections 6 and 7 show that the first order solution tends, within the margin of precision of the numerical procedure, to the asymptotic field distribution corresponding to a crack growing in an isotropic elastic material. A qualitative explanation of this effect can be the following. In the pure kinematic-hardening limit, the yield surface is subject to a pure translation in stress space during plastic deformation. Due to the stress singularity, the stress and the back stress tend to infinity and their difference, the reduced stress, becomes negligible, compared to these. This produces a behavior similar to an elastic material. These observations were precisely confirmed by Bigoni and Radi (1996), where an analytical second order solution was given for Mode III propagation in a J_2-flow theory material, obeying pure kinematic hardening. In particular, it has been shown that the first order asymptotic solution is coincident with the asymptotic solution of a crack growing in an isotropic elastic material, having elastic shear modulus equal to the plastic modulus in shear. In the present case of Gurson elastoplastic model, a second order asymptotic solution based on the stress representation of Bigoni and Radi (1996) needs more investigation.

4. MODE I BOUNDARY CONDITIONS

Mode I symmetry conditions render the analysis of the interval $0 \leqslant \vartheta \leqslant \pi$ sufficient and, together with the regularity assumption for the stress and velocity functions,

imply the vanishing of the non-symmetric stress and velocity functions along the symmetry plane at $\vartheta = 0$ [see Bose and Ponte Castañeda (1992) for a detailed discussion on regularity conditions]

$$w_\vartheta(0) = T_{r\vartheta}(0) = 0,$$
$$w_{r,\vartheta}(0) = T_{rr,\vartheta}(0) = T_{\vartheta\vartheta,\vartheta}(0) = T_{33,\vartheta}(0) = 0. \tag{4.1}$$

Two additional boundary conditions are given by the vanishing of the traction $\mathbf{T}\mathbf{e}_\vartheta$ on the crack surfaces at $\vartheta = \pi$

$$T_{\vartheta\vartheta}(\pi) = T_{r\vartheta}(\pi) = 0. \tag{4.2}$$

Moreover, a non-singular behavior of the angular functions $\boldsymbol{\Sigma}$, $\boldsymbol{\Omega}$ and $\boldsymbol{\Sigma}_F$ is assumed at $\vartheta = 0$, which implies from (3.6)

$$\boldsymbol{\Sigma}(0) = -s\mathbf{T}(0), \quad \boldsymbol{\Omega}(0) = -s\mathbf{A}(0), \quad \boldsymbol{\Sigma}_F(0) = -sT_F(0). \tag{4.3}$$

By substituting these initial data into relations (3.16) and (3.17) one finds

$$\mathbf{A}(0) = (1-b)\frac{\mathbf{Q}(0)\cdot\mathbf{T}(0)}{\mathbf{Q}(0)\cdot[\mathbf{T}(0)-\mathbf{A}(0)]}[\mathbf{T}(0)-\mathbf{A}(0)], \tag{4.4}$$

$$\mathbf{Q}(0)\cdot\mathbf{A}(0) = (1-b)\mathbf{Q}(0)\cdot\mathbf{T}(0), \tag{4.5}$$

whence a substitution of (4.5) into (4.4) gives

$$\mathbf{A}(0) = (1-b)\mathbf{T}(0), \tag{4.6}$$

and therefore

$$\tilde{\mathbf{T}}(0) = \mathbf{T}(0) - \mathbf{A}(0) = b\mathbf{T}(0). \tag{4.7}$$

Observe that at $\vartheta = 0$, $\mathbf{e}_r = \mathbf{e}_1$ and $\mathbf{e}_\vartheta = \mathbf{e}_2$. Therefore, tensor $\mathbf{T}$ can be written at $\vartheta = 0$ in the form

$$\mathbf{T}(0) = T_{rr}(0)\mathbf{e}_1 \otimes \mathbf{e}_1 + T_{\vartheta\vartheta}(0)\mathbf{e}_2 \otimes \mathbf{e}_2 + T_{33}(0)\mathbf{e}_3 \otimes \mathbf{e}_3. \tag{4.8}$$

By using the boundary conditions (4.1) and the equilibrium equation (3.8_1) evaluated at $\vartheta = 0$ [see (A1.5) of Appendix 1], the tensor $\mathbf{T}'(0)$ reduces to

$$\mathbf{T}'(0) = -sT_{rr}(0)(\mathbf{e}_2 \otimes \mathbf{e}_1 + \mathbf{e}_1 \otimes \mathbf{e}_2). \tag{4.9}$$

Moreover, by using the boundary conditions (4.1), the values at $\vartheta = 0$ of the vector $\mathbf{w}$ and its derivative $\mathbf{w}'$ [see (A1.6) of Appendix 1], can be cast in the form

$$\mathbf{w}(0) = w_r(0)\mathbf{e}_1, \tag{4.10}$$

$$\mathbf{w}'(0) = [w_{\vartheta,\vartheta}(0) + w_r(0)]\mathbf{e}_2. \tag{4.11}$$

Then, the constitutive relation (3.15) at $\vartheta = 0$ becomes

$$[w_{\vartheta,\vartheta}(0) + w_r(0)]\mathbf{e}_2 \otimes \mathbf{e}_2 + sw_r(0)\mathbf{e}_1 \otimes \mathbf{e}_1 = -s^2[(1+\nu)\mathbf{T}(0) - \nu\,\mathrm{tr}\,\mathbf{T}(0)\mathbf{I}] + s\lambda(0)\mathbf{Q}(0), \tag{4.12}$$

where $\mathbf{Q}(0)$ and $\lambda(0)$ may be evaluated from (3.12) and (3.13) by using conditions (4.3_1) and (4.7)

$$\mathbf{Q}(0) = \frac{3b}{2T_{\mathrm{F}}(0)}\operatorname{dev}\mathbf{T}(0) + \gamma(0)\mathbf{I}, \quad \gamma(0) = \frac{\phi}{2}\sinh\left(\frac{\operatorname{tr}\mathbf{T}(0)}{2T_{\mathrm{F}}(0)}b\right), \tag{4.13}$$

$$\lambda(0) = -s\frac{(1-\phi)T_{\mathrm{F}}^2(0)}{3h_{\mathrm{m}}b^2\left[\dfrac{3b|\operatorname{dev}\mathbf{T}(0)|^2}{2T_{\mathrm{F}}(0)} + \gamma(0)\operatorname{tr}\mathbf{T}(0)\right]}. \tag{4.14}$$

Since all the assigned boundary conditions (4.1) and (4.2) are of homogeneous type, the normalization condition $T_{\vartheta\vartheta}(0) = 1$ is adopted to avoid the trivial solution.

In order to solve the system (3.15)–(3.17) of ODEs, the Runge–Kutta procedure is used. This approach requires the knowledge of the values $\mathbf{w}(0)$, $\mathbf{T}(0)$, $\mathbf{A}(0)$ and $T_{\mathrm{F}}(0)$. The boundary conditions together with the system (3.15)–(3.17) evaluated at $\vartheta = 0$, do not specify the value of $T_{\mathrm{rr}}(0)$. Therefore, the integration is performed by assuming arbitrary initial values for $T_{\mathrm{rr}}(0) = p$ and s. On the basis of a check on the final values $T_{\vartheta\vartheta}(\pi)$ and $T_{\mathrm{r}\vartheta}(\pi)$, the guessed values of p and s are reassigned and the process is iterated using a modified Powell hybrid method, until $T_{\vartheta\vartheta}(\pi)$ and $T_{\mathrm{r}\vartheta}(\pi)$ are found to be sufficiently close to zero. The values of $T_{33}(0)$ and $T_{\mathrm{F}}(0)$ may be found by solving the non-linear algebraic system of equations† formed by the plane strain condition and the yield condition at $\vartheta = 0$

$$-s\{T_{33}(0) - \nu[T_{\mathrm{rr}}(0) + T_{\vartheta\vartheta}(0)]\} + \lambda(0)\mathrm{Q}_{33}(0) = 0, \tag{4.15}$$

$$\frac{3|\operatorname{dev}\mathbf{T}(0)|^2}{2T_{\mathrm{F}}^2(0)}b^2 + 2\phi\cosh\left(\frac{\operatorname{tr}\mathbf{T}(0)}{2T_{\mathrm{F}}(0)}b\right) = 1 + \phi^2. \tag{4.16}$$

When $T_{33}(0)$ and $T_{\mathrm{F}}(0)$ are known, $w_{\mathrm{r}}(0)$ and $w_{\vartheta,\vartheta}(0)$ may be derived from (4.12)

$$w_{\mathrm{r}}(0) = -s\{T_{\mathrm{rr}}(0) - \nu[T_{\vartheta\vartheta}(0) + T_{33}(0)]\} + \lambda(0)\mathrm{Q}_{\mathrm{rr}}(0), \tag{4.17}$$

$$w_{\vartheta,\vartheta}(0) = -w_{\mathrm{r}}(0) - s^2\{T_{\vartheta\vartheta}(0) - \nu[T_{\mathrm{rr}}(0) - T_{33}(0)]\} + s\lambda(0)\mathrm{Q}_{\vartheta\vartheta}(0). \tag{4.18}$$

Conditions (4.1), (4.6), (4.15)–(4.17) give all the components of vector $\mathbf{y}(0)$.

4.1. *Series expansions at* $\vartheta = 0$

The governing system of (3.23) has a singularity at $\vartheta = 0$ and at $\vartheta = \pi$, due to the term $\sin\vartheta$ multiplying the higher order derivative. The singularity at $\vartheta = \pi$ does not create problems for numerical solution. The solution is in fact well-behaved near $\vartheta = \pi$, and thus the numerical integration can be performed to an angle $\pi - \varepsilon$ as close to π as needed to satisfy any required precision. In order to avoid the numerical difficulty at $\vartheta = 0$, the integration of (3.23) must be initiated from a small value, say ε, of ϑ. Therefore, the values of the unknown functions in $\mathbf{y}$ at a small ε must

† Integration of the ODEs system (3.23) has been performed using Runge–Kutta–Verner method, and iterations for satisfying boundary conditions at $\vartheta = \pi$ were performed using the modified Powell hybrid algorithm. These were available in the IMSL Library (Subroutines DIVPRK and DNEQNF). The non-linear system (4.17)–(4.18) was solved by using Subroutine DNEQNJ of the IMSL Library.

be evaluated. These values are obtained in Appendix 2, by performing asymptotic expansions of the unknown fields ahead of the crack tip. In particular, we obtain the following values of the stress components at $\vartheta = \varepsilon$

$$\begin{aligned} T_{r\vartheta}(\varepsilon) &= \varepsilon[T_{\vartheta\vartheta}(0) - (s+1)T_{rr}(0)] + o(\varepsilon), \\ T_{rr}(\varepsilon) &= T_{rr}(0) + o(\varepsilon), \\ T_{\vartheta\vartheta}(\varepsilon) &= T_{\vartheta\vartheta}(0) + o(\varepsilon), \\ T_{33}(\varepsilon) &= T_{33}(0) + o(\varepsilon). \end{aligned} \tag{4.19}$$

When (A2.13) is multiplied by the unit vectors (A2.15), we obtain the Taylor series expansion of the back stress components

$$\begin{aligned} A_{r\vartheta}(\varepsilon) &= \varepsilon(1-b)\left[T_{\vartheta\vartheta}(0) + \left(\frac{s^2}{b-s} - 1\right)T_{rr}(0)\right] + o(\varepsilon), \\ A_{rr}(\varepsilon) &= (1-b)T_{rr}(0) + o(\varepsilon), \\ A_{\vartheta\vartheta}(\varepsilon) &= (1-b)T_{\vartheta\vartheta}(0) + o(\varepsilon), \\ A_{33}(\varepsilon) &= (1-b)T_{33}(0) + o(\varepsilon). \end{aligned} \tag{4.20}$$

From the Taylor series expansion (A2.2) of $\mathbf{w}$, the velocity functions at $\vartheta = \varepsilon$ may be determined

$$w_r(\varepsilon) = w_r(0) + o(\varepsilon), \quad w_\vartheta(\varepsilon) = \varepsilon w_{\vartheta,\vartheta}(0) + o(\varepsilon), \tag{4.21}$$

$w_r(0)$ and $w_{\vartheta,\vartheta}(0)$ being known from (4.17) and (4.18). Finally, (A2.14) gives the Taylor series expansion for T_F.

All the values of the unknown functions in $\mathbf{y}(\varepsilon)$ are now determined within an error lower than ε, and the numerical solution of problem (3.23) can be obtained by starting the integration at $\vartheta = \varepsilon$, rather than at $\vartheta = 0$.

Finally, all results are normalized through the condition $T_F(\vartheta_1) = 1$, so as to facilitate comparisons with Ponte Castañeda (1987) and Radi and Bigoni (1994).

It is important to remark that all the equations reported in the present section are referred to plane strain. The plane stress case can easily be obtained simply by introducing the conditions $T_{33} = A_{33} = 0$ in all the previous equations. In Sections 6 and 7, results referring to plane strain and plane stress are presented. The next section is dedicated to a detailed analysis on continuity of stress fields at the crack tip.

5. CONTINUITY CONDITIONS AND TRANSITION OF HARDENING TYPE

Discontinuities in stress and velocity fields may in general occur in the framework of plasticity [see, e.g., Brannon and Drugan (1993) and references cited therein]. For the steady-state crack propagation problem, discontinuities in the asymptotic stress field may exist across radial lines emanating from the crack tip. In particular, the stress components σ_{rr} and σ_{33} only may suffer jumps, since continuity of the tractions

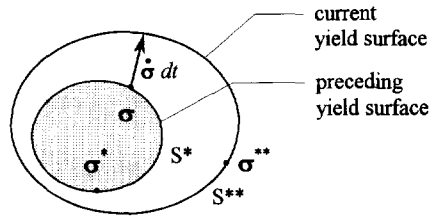

Fig. 3. Subsequent yield surfaces.

are implied by quasistatic equilibrium condition. Drugan and Rice (1984) proved a sufficient condition to exclude these stress jumps for elastoplastic materials with associative flow-rule, and any type of hardening behavior for which the current yield locus fully incorporates all preceding yield loci. Drugan (1995) has recently extended the constitutive range of validity of this proof; it now contains as a subclass all types of response analysed in the present paper. In the case of the Gurson model considered in the present paper, we show that for the mixed hardening parameter b greater than the transition value 0.5, all the subsequent yield surfaces contain the preceding. Although Drugan's (1995) new analysis applies for all b values, and all of our solutions are completely continuous regardless of b-value, this transition value is interesting as it seems to coincide with the appearance of a region of rapid field variation in our solution.

In order to obtain the transition value of the mixed hardening parameter b, let us denote by $\boldsymbol{\sigma}$ and $\boldsymbol{\sigma}^*$ two generic stress states, which belong to the yield surface $\mathscr{S}^*$ at time t (Fig. 3).

$$f(\boldsymbol{\sigma}^*, \boldsymbol{\alpha}, \sigma_F) = f(\boldsymbol{\sigma}, \boldsymbol{\alpha}, \sigma_F) = 0. \tag{5.1}$$

The stress increment from the initial state at time t, described by the state variables $\boldsymbol{\sigma}$, $\boldsymbol{\alpha}$ and σ_F, to the final state at $t+\mathrm{d}t$, is denoted by $\dot{\boldsymbol{\sigma}}\,\mathrm{d}t$. If this increment satisfies plastic unloading or neutral loading conditions, the yield surface remains frozen. Otherwise, for $\Lambda > 0$, the hardening variables are incremented by $\dot{\boldsymbol{\alpha}}\,\mathrm{d}t$ and $\dot{\sigma}_F\,\mathrm{d}t$, where the material derivatives are the functions (2.16) of the stress $\boldsymbol{\sigma}$ and stress rate $\dot{\boldsymbol{\sigma}}$. As a consequence of the increment of hardening variables, the yield surface expands and translates in stress space ($\mathscr{S}^{**}$ in Fig. 3) and the elastic domain becomes the set of all the stress states $\boldsymbol{\sigma}^{**}$ satisfying the condition

$$f(\boldsymbol{\sigma}^{**}, \boldsymbol{\alpha}+\dot{\boldsymbol{\alpha}}\,\mathrm{d}t, \sigma_F+\dot{\sigma}_F\,\mathrm{d}t) \leqslant 0. \tag{5.2}$$

Therefore, the yield locus at $t+\mathrm{d}t$ fully incorporates the yield locus at t, if, for every $\boldsymbol{\sigma}$ and $\boldsymbol{\sigma}^*$ satisfying (5.1), $\boldsymbol{\sigma}^*$ satisfies (5.2), too, i.e.

$$f(\boldsymbol{\sigma}^*, \boldsymbol{\alpha}+\dot{\boldsymbol{\alpha}}\,\mathrm{d}t, \sigma_F+\dot{\sigma}_F\,\mathrm{d}t) \leqslant 0, \quad \forall\, \boldsymbol{\sigma}, \boldsymbol{\sigma}^* \in \mathscr{S}^*. \tag{5.3}$$

A Taylor series expansion of f near $\boldsymbol{\sigma}^*$, $\boldsymbol{\alpha}$ and σ_F yields

$$f(\boldsymbol{\sigma}^*, \boldsymbol{\alpha}+\dot{\boldsymbol{\alpha}}\,\mathrm{d}t, \sigma_F+\dot{\sigma}_F\,\mathrm{d}t) = f(\boldsymbol{\sigma}^*, \boldsymbol{\alpha}, \sigma_F) + \left[\dot{\boldsymbol{\alpha}} \cdot \left.\frac{\partial f}{\partial \boldsymbol{\alpha}}\right|_{(\boldsymbol{\sigma}^*, \boldsymbol{\alpha}, \sigma_F)} + \dot{\sigma}_F \left.\frac{\partial f}{\partial \sigma_F}\right|_{(\boldsymbol{\sigma}^*, \boldsymbol{\alpha}, \sigma_F)}\right]\mathrm{d}t + o(\mathrm{d}t). \tag{5.4}$$

By using (5.1) and (2.16) in (5.4), and neglecting higher order terms in dt, condition (5.3) becomes

$$\mathbf{Q}^* \cdot [(b-1)\tilde{\boldsymbol{\sigma}} - b\tilde{\boldsymbol{\sigma}}^*] \leqslant 0, \quad \forall \boldsymbol{\sigma}, \boldsymbol{\sigma}^* \in \mathscr{S}^*, \tag{5.5}$$

where

$$\mathbf{Q}^* = \frac{3}{2\sigma_F} \operatorname{dev} \tilde{\boldsymbol{\sigma}}^* + \frac{\phi}{2} \sinh\left(\frac{\operatorname{tr} \tilde{\boldsymbol{\sigma}}^*}{2\sigma_F}\right) \mathbf{I}. \tag{5.6}$$

It is possible to find the maximum value of the left hand side of inequality (5.5), for $\boldsymbol{\sigma}$ satisfying the yield condition (5.1), by employing the technique of Lagrangian multipliers

$$\max_{\tilde{\boldsymbol{\sigma}}, \xi} \{\mathbf{Q}^* \cdot [(b-1)\tilde{\boldsymbol{\sigma}} - b\tilde{\boldsymbol{\sigma}}^*] - \xi f(\boldsymbol{\sigma}, \boldsymbol{\alpha}, \sigma_F)\} \leqslant 0, \quad \forall \boldsymbol{\sigma}^* \in \mathscr{S}^*, \tag{5.7}$$

where ξ is a Lagrangian multiplier. From problem (5.7) the following extremum condition can be obtained

$$(b-1)\mathbf{Q}^* = \xi \mathbf{Q}, \quad \forall \boldsymbol{\sigma}, \boldsymbol{\sigma}^* \in \mathscr{S}^*. \tag{5.8}$$

The admissible solutions of (5.8) are $\xi = \pm(b-1)$, since $\mathbf{Q}$ is one to one with the stress state $\boldsymbol{\sigma}$ on the yield surface, so that $\mathbf{Q}^* = \pm\mathbf{Q}$ and correspondingly $\tilde{\boldsymbol{\sigma}}^* = \pm\tilde{\boldsymbol{\sigma}}$. It is easy to see that the maximum is achieved when these relations are taken with the minus sign. Finally, we obtain that for $b \geqslant 0.5$ inequality (5.5) is always satisfied, and this condition holds true regardless of the value of porosity, and, therefore, it is also valid for von Mises yield surface.

6. PLANE STRAIN: RESULTS

Values of the singularity (s), elastic unloading (ϑ_1) and reloading (ϑ_2) angles are reported in Tables 1 and 2 for different values of porosity (ϕ) and hardening parameter b. Tables 1 and 2 refer to $\alpha_G = 0.001$ and $\alpha_G = 0.1$, respectively. For conciseness, only the value $\nu = 1/3$ has been considered.

The angular distribution of components of functions $\mathbf{T}$, $\mathbf{A}$, T_F and $\mathbf{w}$ are plotted in Figs 4–9, for different values of mixity parameter b and small and high strain hardening ($\alpha_G = 0.001$, in Figs 4–6, and $\alpha_G = 0.1$, in Figs 7–9). Functions $\mathbf{w}$, $\mathbf{T}$, $\mathbf{A}$ represent, aside from an amplitude factor, the asymptotic near-tip velocity, stress and back stress fields, respectively. The cases $\phi = 0$ (J_2-flow theory), $\phi = 0.01$, and $\phi = 0.05$ are investigated. First of all, it is important to note the strong effects of the hardening modulus and porosity, which were already known from the isotropic hardening case. On comparison of the cases relative to $b = 0.8$ (hardening almost isotropic) and $b = 0.1$ (hardening almost kinematic), the effect of anisotropic hardening is evident. The out-of-plane, radial and circumferential stress components, which tend to coalesce for $b = 0.8$ in the central zone of the graphs, tend to separate when b decreases, and the angular distribution of components of $\mathbf{A}$ clearly tend to the angular distribution of components of $\mathbf{T}$. Moreover, the elastic sector behind the crack tip becomes very thin, compared to the elastic sector for isotropic hardening. More significant effects

Table 1. *Values of the singularity exponent s and angles ϑ_1 and ϑ_2, for $\nu = 1/3$ and $\alpha_G = 0.001$, for different values of mixed hardening parameter b and porosity ϕ, under plane strain conditions*

ϕ		0			0.01			0.05	
b	s	ϑ_1	ϑ_2	s	ϑ_1	ϑ_2	s	ϑ_1	ϑ_2
1.00	−0.056399	136.965	138.444	−0.032244	132.885	142.724	−0.027462	97.471	178.510
0.90	−0.06290	138.290	139.665	−0.037823	135.156	140.000	−0.024814	113.240	169.017
0.80	−0.071557	139.985	141.393	−0.046535	137.247	139.520	−0.025974	130.746	148.535
0.70	−0.083501	142.258	143.780	−0.059498	139.794	141.159	−0.034884	136.597	141.484
0.60	−0.100554	145.373	147.021	−0.078673	143.334	144.800	−0.051840	141.102	142.502
0.50	−0.125850	149.720	151.450	−0.107332	148.423	150.099	−0.081542	147.477	149.019
0.40	−0.164048	155.574	157.288	−0.150049	155.163	156.879	−0.129769	155.766	157.481
0.30	−0.220475	162.736	164.287	−0.211037	162.715	164.267	−0.198068	163.784	165.311
0.20	−0.298421	170.281	171.504	−0.292593	170.392	171.607	−0.285528	171.092	172.260
0.10	−0.395688	176.997	177.706	−0.392258	177.143	177.837	−0.389071	177.480	178.129

Table 2. *Values of the singularity exponent s and angles* ϑ_1 *and* ϑ_2, *for* $\nu = 1/3$ *and* $\alpha_G = 0.1$, *for different values of mixed hardening parameter b and porosity* ϕ, *under plane strain conditions*

ϕ		0			0.05	
b	s	ϑ_1	ϑ_2	s	ϑ_1	ϑ_2
1.00	−0.20956	122.012	175.318	−0.26382	94.585	
0.80	−0.20412	130.627	168.299	−0.23375	104.951	
0.60	−0.21107	140.298	162.949	−0.20119	126.776	175.582
0.40	−0.23711	151.959	164.083	−0.21079	152.769	165.185
0.20	−0.32727	167.656	176.021	−0.31581	168.644	176.597
0.10	−0.40934	176.012	179.996	−0.40336	176.527	

of anisotropic hardening can be appreciated from Figs 10 and 11, which demonstrate the effects of hardening mixity on field singularity and thickness of elastic sector in the crack wake. In particular, Fig. 10 shows that the singularity decreases with porosity and in any case tends to the value −0.50 when the isotropic component of hardening tends to vanish. Figure 11 refers to $\phi = 0$, 0.01, and 0.05, respectively. In these figures the amplitude of the unloading and reloading angles are reported as functions of b. The porosity is seen to produce an increase in the thickness of the elastic sector, whereas an opposite effect is related to an increase in the kinematic component of hardening. Moreover, the elastic sector moves toward $\vartheta = \pi$, when the mixity parameter b decreases. The above results may have the following qualitative explanation: in the case of pure kinematic hardening, during the plastic history of the near-tip particle, the yield surface translates in stress space without any modification in size. Therefore, compared to the isotropic-hardening case, the elastic path of the particle is extremely short, the energy dissipation during a loading–reloading cycle is small, and the material remains almost always on the plastic branch of constitutive equation. In conclusion, a thin elastic sector results and the singularity approaches the value −0.5, corresponding to a linear constitutive equation. The tendency of $\tilde{\mathbf{T}}$ to zero, the tendency of the singularity to the value −0.5, and the decrease of the elastic sector, when the mixity parameter b approaches 0, induce to the conjecture that the solution corresponds to the asymptotic fields relative to a crack steadily running in an isotropic linear elastic medium, in the limit of pure kinematic hardening. This conjecture was indeed analytically confirmed in the case of Mode III propagation in a J_2-material (Bigoni and Radi, 1996).

It can be finally observed from Figs 4 and 5 that the out-of-plane and radial stress components develop a (continuous) rapid variation across the elastic sector, when b decreases below the transition value 0.5, i.e. the value at which the material hardening alters so that the current yield locus no longer incorporates all prior yield loci (see Section 5). The continuity of the variation of the stress components can be appreciated in Fig. 12, where the detail of the rapid variation of Fig. 4, relative to $b = 0.4$, is reported. It should be noted that the more the kinematic component of hardening is high, the more the variation is steep. Moreover, an increase in the porosity, or in the hardening modulus, tends to eliminate this effect (in Figs 7 and 8, relative to $\alpha_G = 0.1$ the rapid variations are absent).

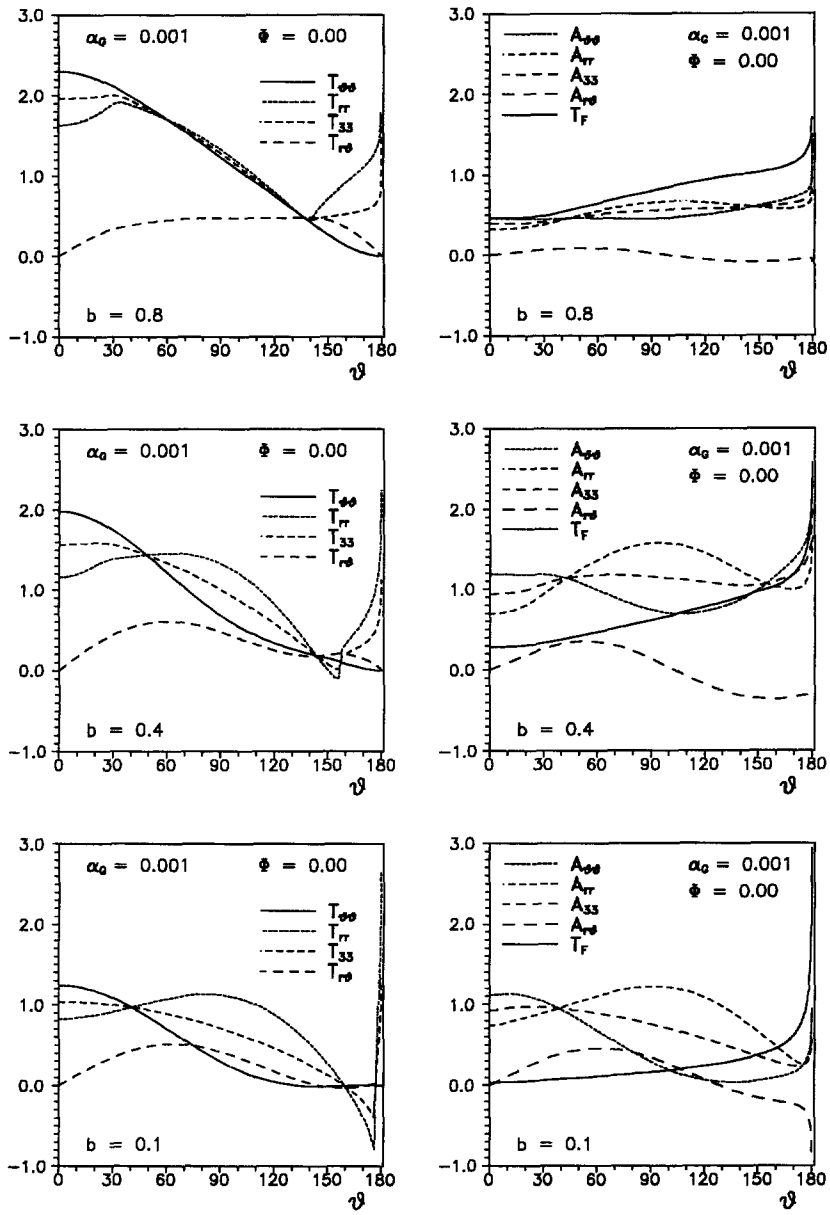

Fig. 4. Angular distribution of stress functions near crack tip for small hardening of the matrix material ($\alpha_G = 0.001$), corresponding to different values of the mixity parameter b, plane strain condition. Case $\phi = 0$, J_2-flow theory.

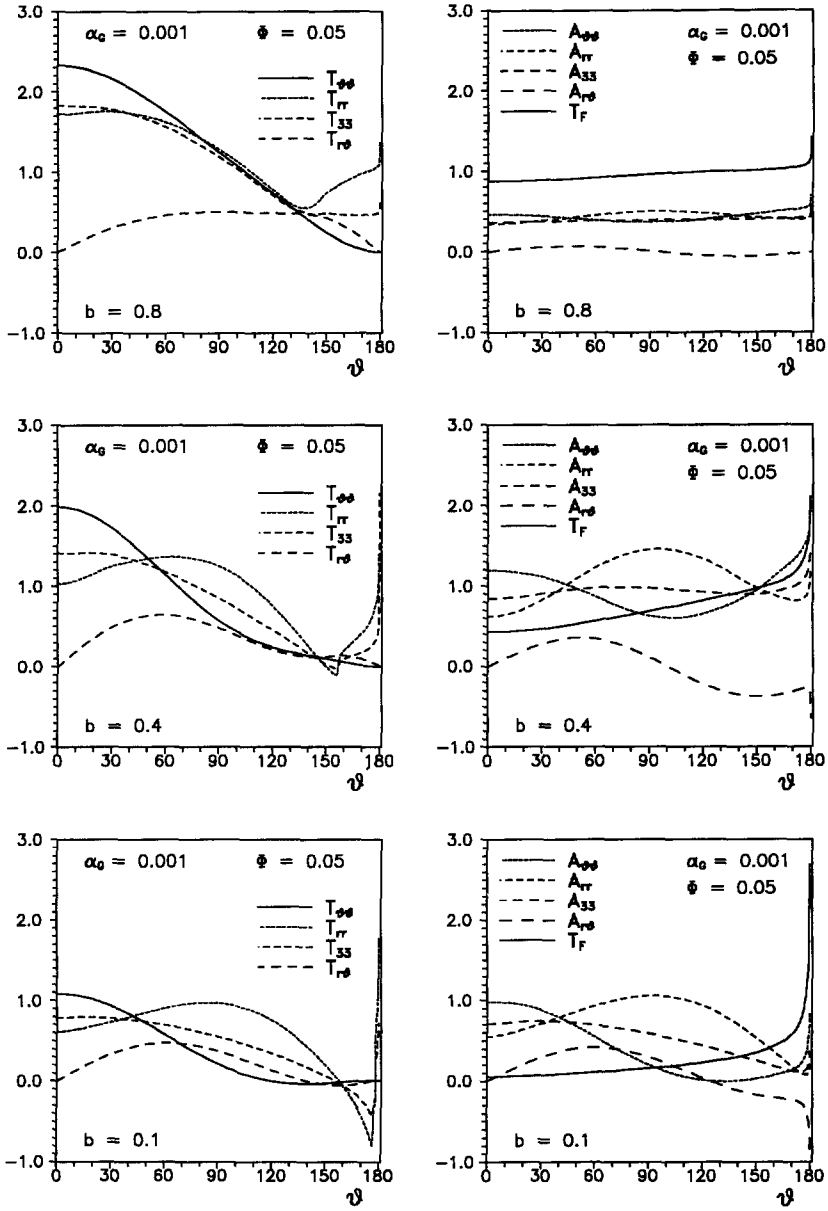

Fig. 5. As for Fig. 4, except that $\phi = 0.05$.

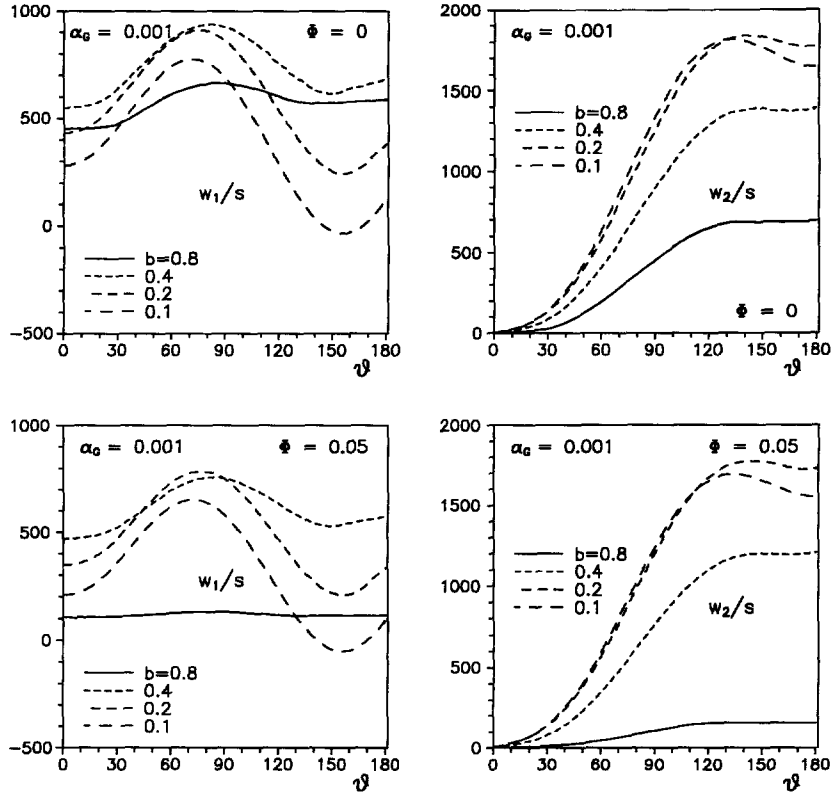

Fig. 6. Near crack-tip velocity functions (normalized with respect to the singularity s) for small hardening of the matrix material ($\alpha_G = 0.001$), for different values of the mixity parameter b, in plane strain conditions. The cases $\phi = 0$ and 0.05 are reported.

In conclusion, anisotropy of hardening and porosity have opposite effects: the former tends to make the unloading sector thin, the singularity high and the angular distribution of fields similar to the elastic case. The latter has an opposite effect, but the limit case of pure kinematic hardening seems to be not influenced by the value of porosity and of hardening modulus.

7. PLANE STRESS: RESULTS

Values of the singularity (s), elastic unloading (ϑ_1) and reloading (ϑ_2) angles are reported in Tables 3 and 4 for different values of porosity (ϕ) and hardening parameter b. Tables 3 and 4 refer to $\alpha_G = 0.001$ and $\alpha_G = 0.1$, respectively. Due to the fact that the Poisson ratio does not influence results, the only value $\nu = 1/2$ has been considered.

The angular distribution of components of functions **T**, **A**, T_F and **w** are plotted in Figs 13 and 14, for $\phi = 0.01$, for different values of mixity parameter b, and small strain hardening ($\alpha_G = 0.001$). In Fig. 15 the singularity s is reported as a function of

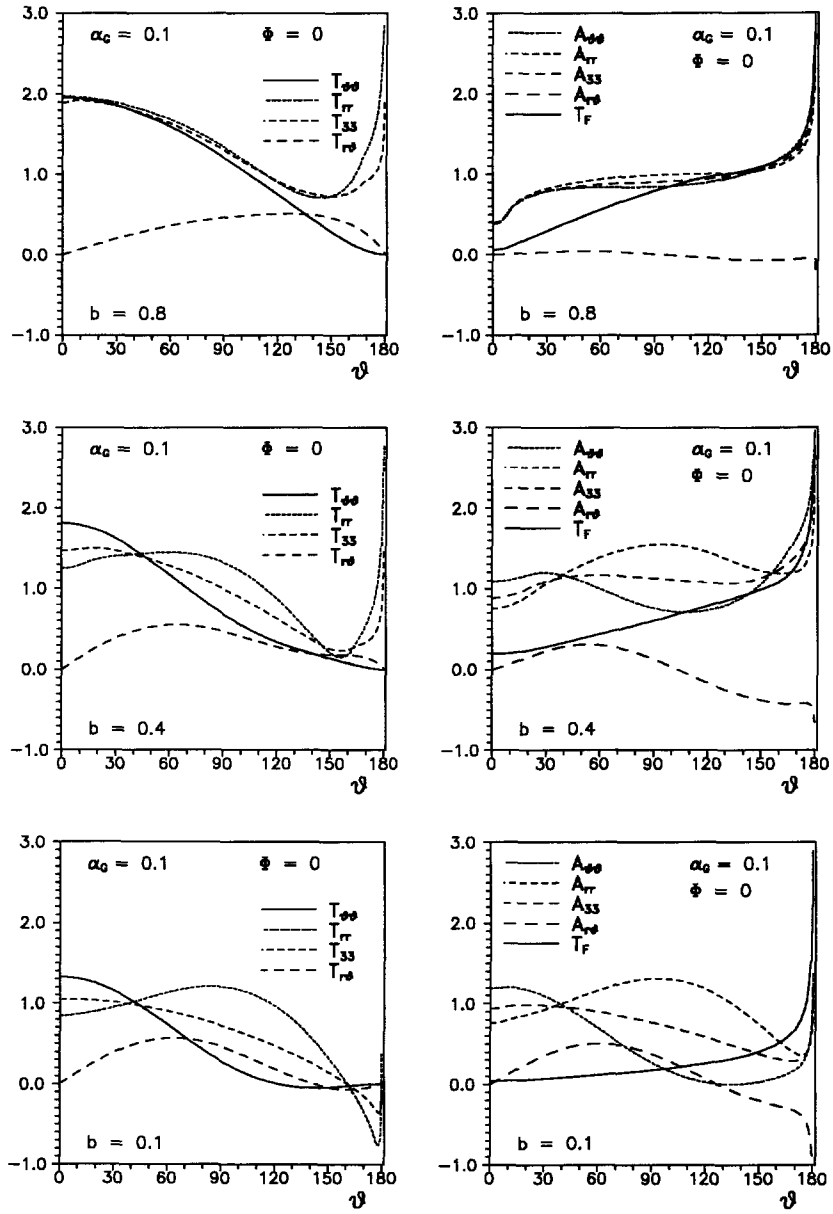

Fig. 7. Angular distribution of stress functions near crack tip for high hardening of the matrix material ($\alpha_G = 0.1$), corresponding to different values of the mixity parameter b, plane strain condition. Case $\phi = 0$, J_2-flow theory.

the mixity parameter b. The amplitude of the elastic sector is plotted, as a function of the parameter b, in Fig. 16. All graphs refer to the case $\phi = 0.01$, because results remain qualitatively unaffected by the porosity [analogously to the isotropic-hardening case of Radi and Bigoni (1994)].

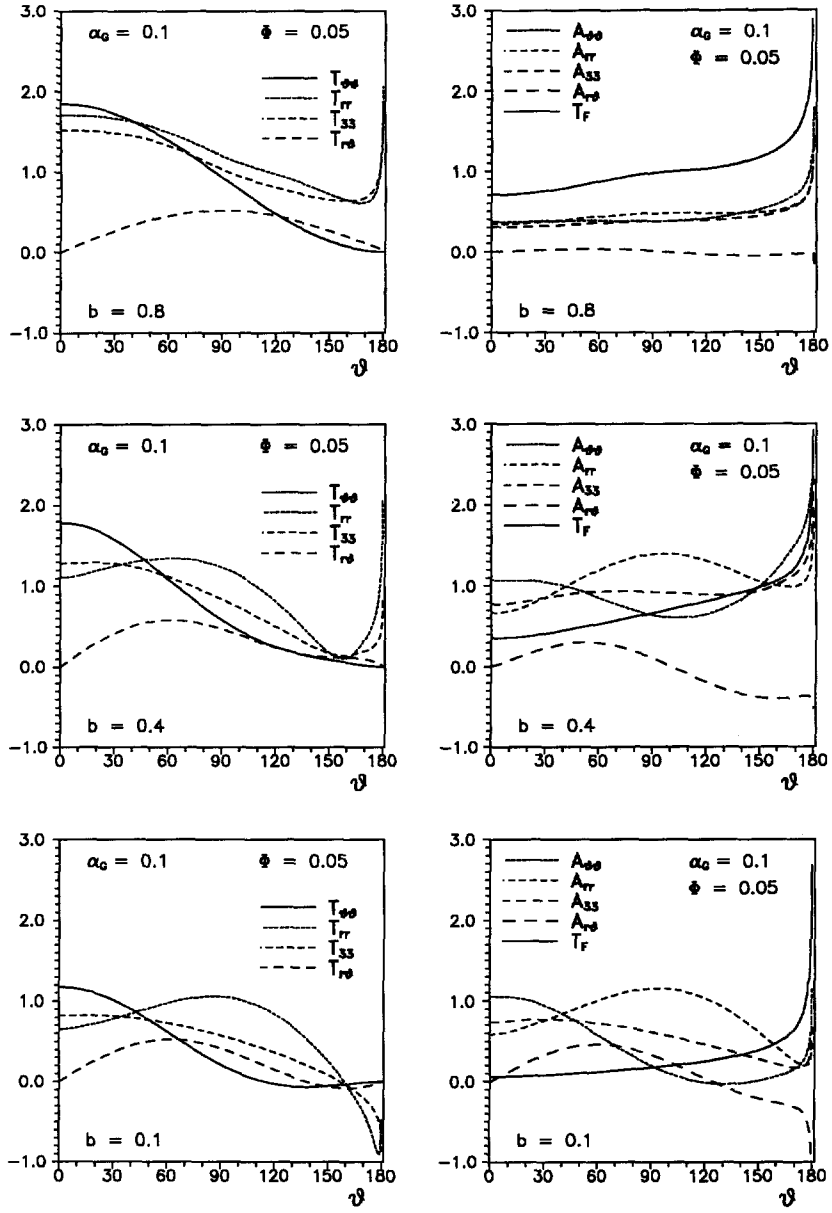

Fig. 8. As for Fig. 7, except that $\phi = 0.05$.

Considerations analogous to the plane strain case can be made and are not repeated here. The principal difference with respect to the plane strain situation is that the elastic sector in the crack wake is of remarkably large size. This was also found by Narasimhan *et al.* (1993), using a finite element technique. It may be important to remark that the unloading sector tends always to zero thickness and moves toward

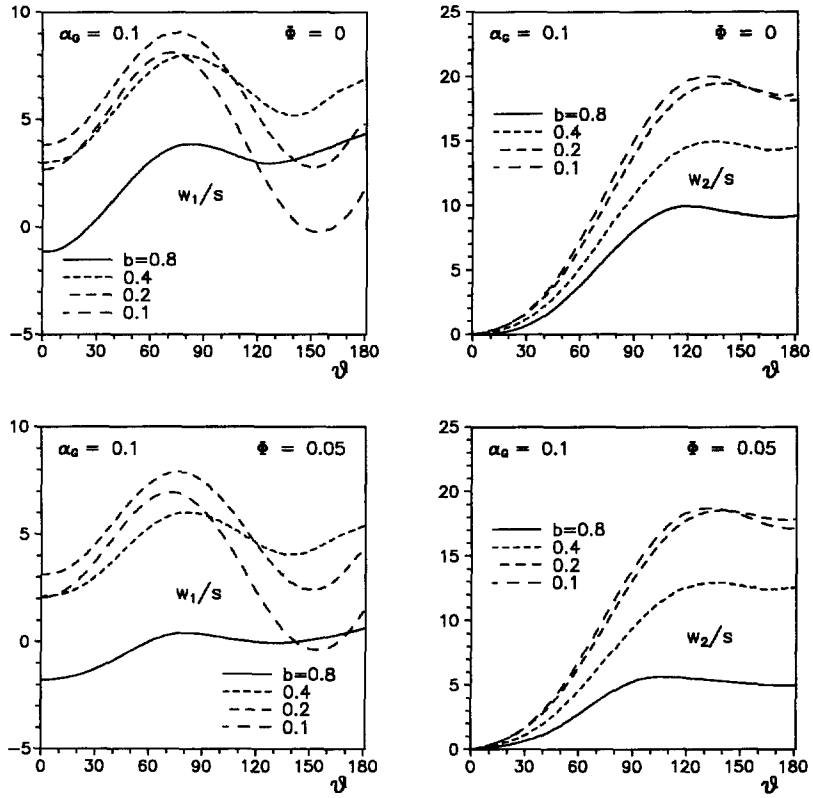

Fig. 9. Near crack-tip velocity functions (normalized with respect to the singularity s) for high hardening of the matrix material ($\alpha_G = 0.1$), for different values of the mixity parameter b, in plane strain conditions. The cases $\phi = 0$ and 0.05 are reported.

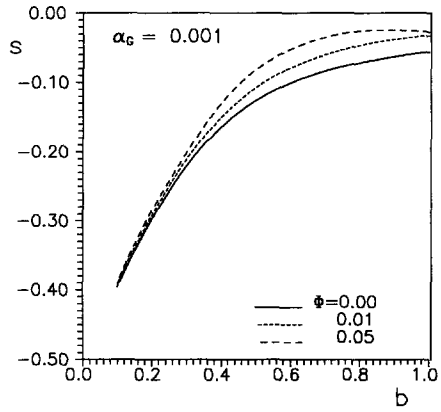

Fig. 10. Strength of the singularity s, as a function of the mixity parameter b, corresponding to the three cases $\phi = 0$, 0.01, and 0.05, in plane strain conditions.

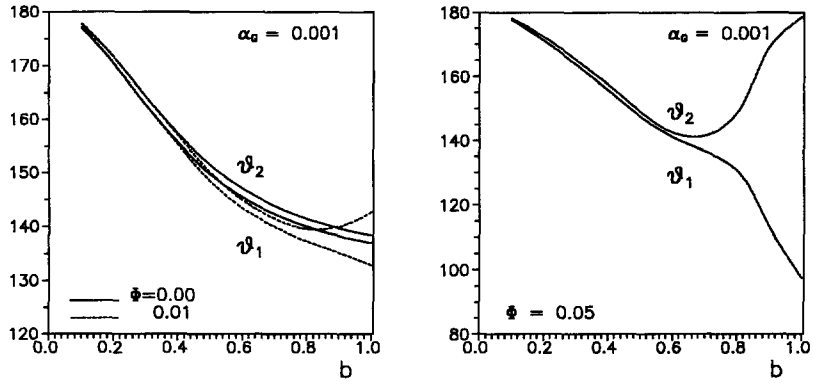

Fig. 11. Elastic unloading and plastic reloading angles, as functions of the mixity parameter b, corresponding to the cases $\phi = 0$, 0.01, and 0.05, in plane strain conditions.

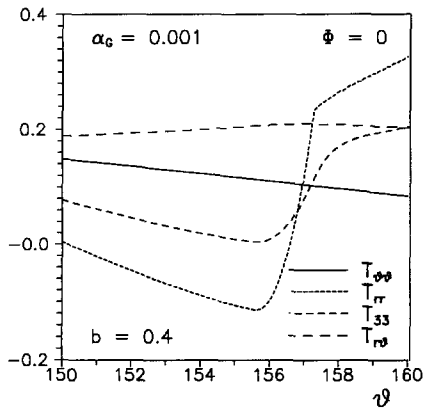

Fig. 12. Particular of Fig. 5: the rapid variation of out-of-plane and radial stress components.

$\vartheta = \pi$, when the limit case of pure kinematic hardening is approached. Note also from Fig. 15, that, differently from the plane strain case, the strength of the singularity, before the dramatic increase toward -0.5, slowly decreases, for b inferior than, approximately, the transition value 0.5. Due to the small influence of porosity on the results, the effect of anisotropic hardening is more apparent here than in the plane strain case.

It may be interesting to note that, in the case of the J_2-flow theory ($\phi = 0$), two elastic sectors appear in the solution for b around the transition value 0.5. This particular feature was found also by Zhang *et al.* (1984), and disappears when the porosity is increased (Table 3).

Finally, it can be noted that the radial stress in the crack wake changes from compressive to tensile when the kinematic component of hardening increases. Therefore, the kinematic component of hardening eliminates the unrealistic effect of compressive radial stress in the crack wake, which seems now to be related to isotropic hardening.

Table 3. *Values of the singularity exponent s and angles* ϑ_1 *and* ϑ_2, *for* $\nu = 1/2$ *and* $\alpha_G = 0.001$, *for different values of mixed hardening parameter b and porosity* ϕ, *under plane stress conditions*

ϕ		0.00			0.01	
b	s	ϑ_1	ϑ_2	s	ϑ_1	ϑ_2
1.00	−0.028664	53.202	179.999	−0.028492	53.034	179.999
0.80	−0.025974	59.965		−0.025830	59.760	
0.60	−0.022122	74.848		−0.022016	74.528	
0.55	−0.020813	83.001	180.000	−0.021324	82.500	
0.50	−0.019313	101.621	158.716	−0.019086	101.319	178.124
		$\vartheta_3 = 172.527$	$\vartheta_4 = 177.022$			
0.45	−0.042199	174.376	176.712	−0.042015	174.933	177.183
0.40	−0.083854	174.328	176.067	−0.083726	174.594	176.300
0.30	−0.177150	174.688	175.905	−0.177095	174.797	176.000
0.20	−0.279683	176.410	177.274	−0.279670	176.461	177.316
0.10	−0.389211	179.201	179.607	−0.389212	179.219	179.619

Table 4. *Values of the singularity exponent s and angles* ϑ_1 *and* ϑ_2, *for* $\nu = 1/2$ *and* $\alpha_G = 0.1$, *for different values of mixed hardening parameter b and porosity* ϕ, *under plane stress conditions*

ϕ		0.00			0.01	
b	s	ϑ_1	ϑ_2	s	ϑ_1	ϑ_2
1.00	−0.23721	73.646		−0.23604	73.476	
0.80	−0.22540	78.558		−0.22431	78.366	
0.60	−0.20614	89.726		−0.20517	89.478	
0.50	−0.19060	106.705		−0.18974	106.335	
0.40	−0.18128	171.908	179.007	−0.18045	172.077	179.118
0.30	−0.22853	172.104	179.111	−0.22799	172.213	179.157

8. CONCLUSIONS

A first order asymptotic solution has been obtained for near-tip fields of a crack quasi-statically growing at constant speed, under Mode I loading conditions, in a material characterized by the mixed isotropic–kinematic strain hardening Gurson incremental elastoplastic model, with constant porosity. This is a generalization of the asymptotic solutions obtained by Miao and Drugan (1995) and Radi and Bigoni (1994) for Gurson model with no hardening and linear isotropic hardening, respectively.

As a consequence of the fact that the material particle approaching the crack tip suffers a strongly non-proportional loading history, the effect of the strain anisotropy has been found significant as (but opposite to) the effects of porosity. Many interesting features have been found, which partially confirm results already known in different

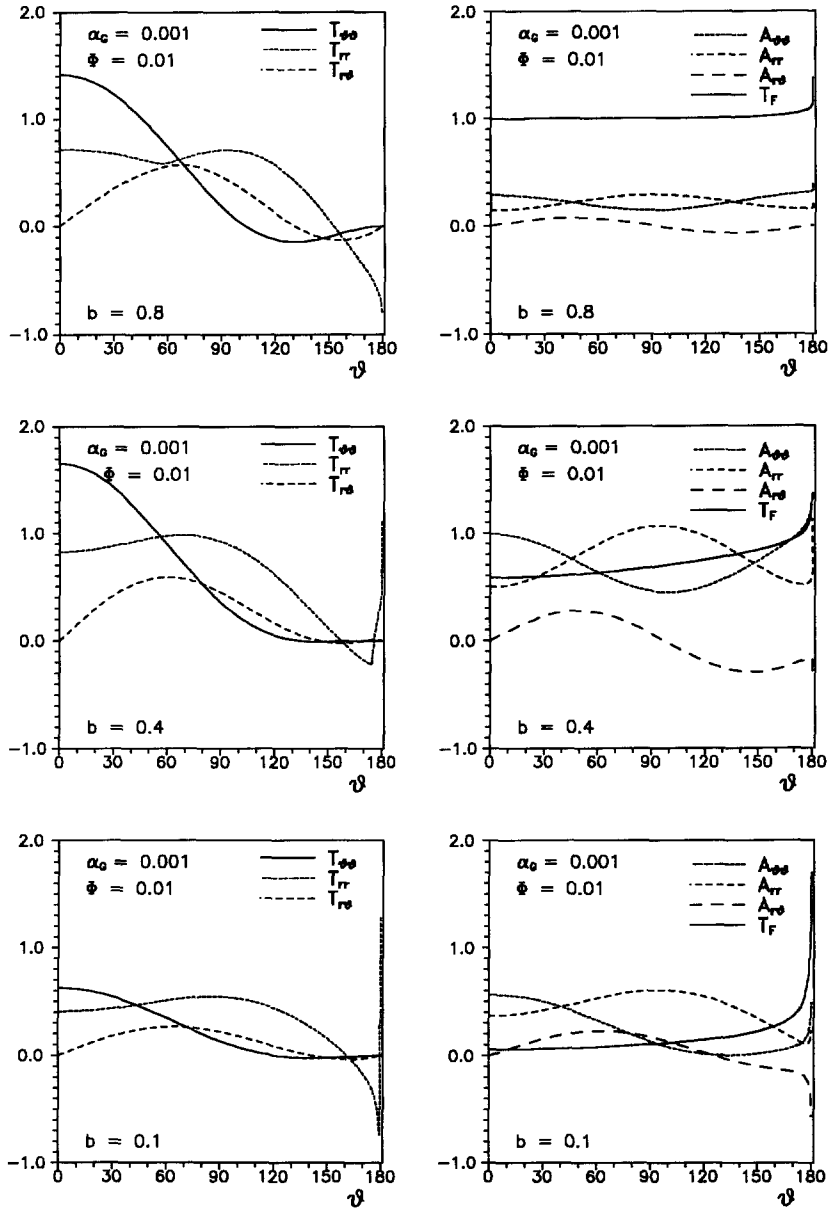

Fig. 13. Angular distribution of stress functions near crack tip for small hardening of the matrix material ($\alpha_G = 0.001$), corresponding to different values of the mixity parameter b, plane stress condition. Case $\phi = 0.01$.

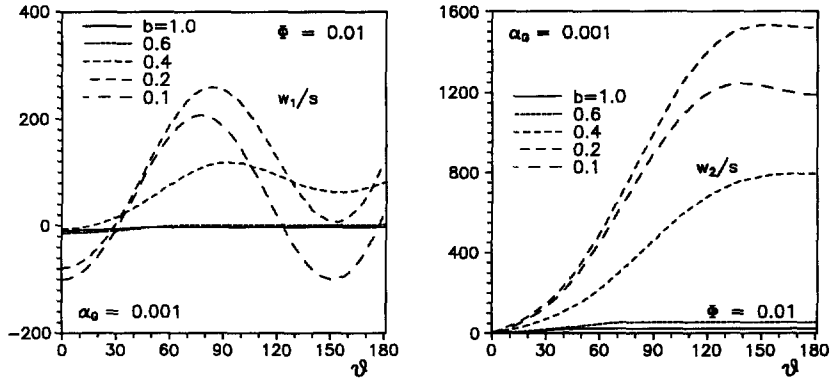

Fig. 14. Near crack-tip velocity functions (normalized with respect to the singularity s) for small hardening of the matrix material ($\alpha_G = 0.001$), for different values of the mixity parameter b, in plane stress conditions. Case $\phi = 0.01$.

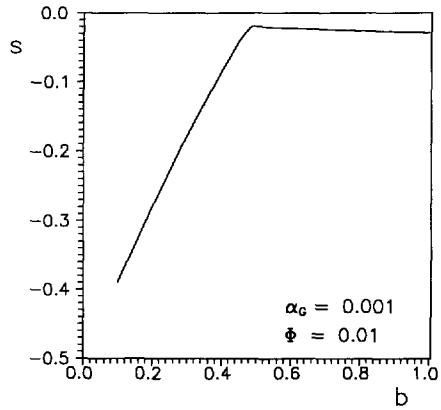

Fig. 15. Strength of the singularity s, as a function of the mixity parameter b, corresponding to the case $\phi = 0.01$, and $\alpha_G = 0.001$, in plane stress conditions.

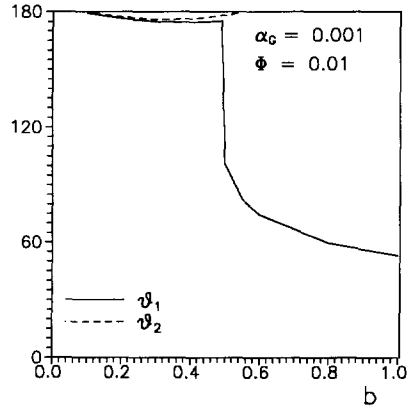

Fig. 16. Elastic unloading and plastic reloading angles, as functions of the mixity parameter b, corresponding to the case $\phi = 0.01$, and $\alpha_G = 0.001$, in plane stress conditions.

contexts (e.g. in Mode III, or for different constitutive equations), and partially are new. In particular:

- An increase in the anisotropic component of hardening leads to a narrow region of elastic unloading. This unloading region occurs much closer to the crack flank when compared to isotropic hardening [in the framework of J_2-flow theory, a similar conclusion was obtained by Delph (1994) and Bigoni and Radi (1996), for Mode III loading conditions, and by Narasimhan and Venkatesha (1993) and Narasimhan *et al.* (1993), using finite element techniques].
- An increase in the anisotropic component of hardening leads to higher values of the singularity strength, which tends to the elastic limit -0.5 when pure kinematic hardening is approached.
- When the pure kinematic hardening limit is approached, the first order representation of reduced stress tends to vanish, and the solution approaches the fields corresponding to propagation in a linear, isotropic elastic material. This apparently occurs independently of the value of porosity. This circumstance was fully confirmed by Bigoni and Radi (1996) in the simple case of Mode III propagation in J_2-flow theory material.
- When the scalar parameter governing the anisotropic component of hardening drops below the transition level 0.5, below which the current yield locus no longer incorporates all prior yield loci, the radial (and out-of-plane, for plane strain) normal stress suffers a rapid variation across the elastic sector.
- As noted by Zhang *et al.* (1984), for plane stress J_2-flow theory, two elastic unloading sectors appear in the solution, when the hardening mixity is close to the transition value. These two sectors coalesce when the porosity is increased.
- For plane stress, isotropic hardening, the radial stress in the plastic sector in the crack wake is compressive (see, e.g., Ponte Castañeda, 1987). This unrealistic effect disappears when the kinematic component of hardening is relevant, and the radial stress becomes tensile.

The fact that an increase in the anisotropic component of hardening produces a strengthening of the singularity suggests the conjecture that the kinematic component of hardening can have an instabilizing effect on crack propagation. On the other hand, an opposed effect is related to an increase of porosity [this latter effect was found by Radi and Bigoni (1994) and Miao and Drugan (1995)].

ACKNOWLEDGEMENTS

The authors wish to acknowledge stimulating discussions with Professor John R. Willis (Cambridge University, U.K.) and Professor Walter J. Drugan (University of Wisconsin-Madison, U.S.A.) in the course of visits financed by the Human Capital and Mobility Programme (Contr. No. CHRX-CT93-0383-DG 12 COMA). D.B. acknowledges the financial support of the Italian Ministry of University and Scientific and Technological Research (MURST).

REFERENCES

Achenbach, J. D., Kanninien, M. F. and Popelar, C. H. (1981) Crack-tip fields for fast fracture of an elastic-plastic material. *J. Mech. Phys. Solids* **29,** 211–225.

Amazigo, J. and Hutchinson, J. W. (1977) Crack-tip fields in steady crack-growth with linear strain hardening. *J. Mech. Phys. Solids* **25,** 81–97.

Aoki, S., Kishimoto, K., Yoshida, T. and Sakata, M. (1987) A finite element study of the near crack tip deformation of a ductile material under mixed mode loading. *J. Mech. Phys. Solids* **35,** 431–455.

Aoki, S., Kishimoto, K. and Takeuchi, N. (1992) An elastic–plastic finite element analysis of a blunting interface crack with microvoid damage. *Int. J. Fracture* **55,** 363–374.

Aravas, N. and McMeeking, R. M. (1985) Microvoid growth and failure in the ligament between a hole and a blunt crack-tip. *Int. J. Fracture* **29,** 21–38.

Beker, R. and Needleman, A. (1986) Effect of yield surface curvature on necking and failure in porous plastic solid. *J. Appl. Mech.* **53,** 491–499.

Bigoni, D. and Radi, E. (1993) Mode I crack propagation in elastoplastic pressure-sensitive materials. *Int. J. Solids Structures* **30,** 899–919.

Bigoni, D. and Radi, E. (1996) Asymptotic solution for Mode III crack growth in J_2-elastoplasticity with mixed isotropic–kinematic strain hardening. *Int. J. Fracture*, in press.

Bose, K. and Ponte Castañeda, P. (1992) Stable crack growth under mixed-mode conditions. *J. Mech. Phys. Solids* **40,** 1053–1103.

Brannon, R. M. and Drugan, W. J. (1993) Influence of non-classical elastic–plastic constitutive features on shock wave existence and spectral solutions. *J. Mech. Phys. Solids* **41,** 297–330.

Delph, T. J. (1994) The steadily propagating viscoplastic crack with elastic unloading. *Int. J. Fracture* **68,** 183–191.

Drugan, J. W. (1995) Private communication.

Drugan, W. J. and Miao, Y. (1992) Influence of porosity on plane strain tensile crack-tip stress fields in elastic-plastic materials: part I. *J. Appl. Mech.* **59,** 559–567.

Drugan, W. J. and Rice, J. R. (1984) Restrictions on quasi-statically moving surfaces of strong discontinuity in elastic-plastic solid. *Mechanics of Material Behavior* (ed. G. J. Dvorak and R. T. Shield), pp. 59–79. Elsevier Press, Amsterdam.

Gurson, A. L. (1977a) Porous rigid–plastic materials containing rigid inclusions—yield function, plastic potential and void nucleation. *Proc. Int. Conf. Fracture* (ed. D. M. R. Taplin), Vol. 2A, pp. 357–364. Pergamon Press, Oxford.

Gurson, A. L. (1977b) Continuum theory of ductile rupture by void nucleation and growth: part I—yield criteria and flow rules for porous ductile media. *Int. J. Engng Mater. Technol.* **99,** 2–15.

Gurtin, M. E. (1981) *An Introduction to Continuous Mechanics*. Academic Press, Harcourt Brace Jovanovich, Publishers.

Hutchinson, J. W. (1968a) Singular behaviour at the end of a tensile crack in a hardening material. *J. Mech. Phys. Solids* **16,** 13–81.

Hutchinson, J. W. (1968b) Plastic stress and strain fields at a crack-tip. *J. Mech. Phys. Solids* **16,** 337–347.

Hutchinson, J. W. (1983a) Fundamentals of the phenomenological theory of non linear fracture mechanics. *J. Appl. Mech.* **50,** 1042–1051.

Hutchinson, J. W. (1983b) Constitutive behavior and crack-tip fields for materials undergoing creep-constrained grain boundary cavitation. *Acta Metall.* **31,** 1079–1088.

Ishizaki, K. and Nanko, M. (1995) A hot isostatic process for fabricating porous materials. *J. Porous Materials* **1,** 19–27.

Jagota, A., Hui, C. Y. and Dawson, P. R. (1987) The determination of fracture toughness for a porous elastic-plastic solid. *Int. J. Fracture* **33,** 111–124.

Lam, P. S. and McMeeking, R. M. (1984) Analyses of steady quasistatic crack growth in plane strain tension in elastic-plastic materials with non-isotropic hardening. *J. Mech. Phys. Solids* **32,** 395–414.

Mear, M. E. and Hutchinson, J. W. (1985) Influence of yield surface curvature on flow localization in dilatant plasticity. *Mech. Mater.* **4,** 395–407.
Miao, Y. and Drugan, W. J. (1993) Influence of porosity on plane strain tensile crack-tip stress fields in elastic-plastic materials: part II. *J. Appl. Mech.* **60,** 883–889.
Miao, Y. and Drugan, J. W. (1995) Asymptotic analysis of growing crack stress/deformation fields in porous ductile metals and implications for stable crack growth. *Int. J. Fracture*, in press.
Narasimhan, R. and Venkatesha, C. S. (1993) A finite element analysis of plane strain dynamic crack growth in materials displaying the Bauschinger effect. *Int. J. Fracture* **61,** 139–157.
Narasimhan, R., Venkatesha, C. S. and Sairam, S. (1993) Quasi-static crack growth in materials displaying the Bauschinger effect—I. Steady-state analysis. *Int. J. Solids Structures* **30,** 659–673.
Needleman, A. and Rice, J. R. (1978) Limits to ductility set by plastic flow localization. *Mechanics of Sheet Metal Forming* (ed. D. P. Koistinien and N. M. Wang), pp. 237–267. Plenum Press, New York.
Needleman, A. and Tvergaard, V. (1987) An analysis of ductile rupture modes at a crack. *J. Mech. Phys. Solids* **35,** 151–183.
Ohno, N. and Hutchinson, J. W. (1984) Plastic flow localization due to non-uniform void distribution. *J. Mech. Phys. Solids* **32,** 63–85.
Östlund, S. and Gudmundson, P. (1988) Asymptotic crack-tip fields for dynamic fracture of linear strain-hardening solids. *Int. J. Solids Structures* **24,** 1141–1148.
Ponte Castañeda, P. (1987) Asymptotic fields in steady crack growth with linear strain-hardening. *J. Mech. Phys. Solids* **35,** 227–268.
Radi, E. and Bigoni, D. (1993) Asymptotic fields of Mode I steady-state crack propagation in non-associative elastoplastic solids. *Mech. Mater.* **14,** 239–251.
Radi, E. and Bigoni, D. (1994) On crack propagation in porous hardening metals. *Int. J. Plasticity* **10,** 761–793.
Rice, J. R. and Rosengren, G. F. (1968) Plane strain deformation near a crack-tip in a power-law hardening material. *J. Mech. Phys. Solids* **16,** 1–12.
Tvergaard, V. (1978) Effect of kinematic hardening on localized necking in biaxially stretches sheets. *Int. J. Mech. Sci.* **20,** 651–658.
Tvergaard, V. (1981) Influence of voids on shear band instabilities under plane strain conditions. *Int. J. Fracture* **17,** 389–407.
Tvergaard, V. (1982) Material failure by void coalescence in localized shear band. *Int. J. Solids Structures* **18,** 659–672.
Tvergaard, V. (1987) Effects of yield surface curvature and void nucleation on plastic flow localization. *J. Mech. Phys. Solids* **35,** 43–60.
Tvergaard, V. (1990) Material failure by void growth to coalescence. *Adv. Appl. Mech.* **27,** 83–151.
Tvergaard, V. and van der Giessen, E. (1991) Effect of plastic spin on localization predictions for a porous ductile material. *J. Mech. Phys. Solids* **39,** 763–781.
Tvergaard, V. and Needleman, A. (1984) Analysis of the cup-cone fracture in a round tensile bar. *Acta Metall.* **32,** 157–169.
Tvergaard, V. and Needleman, A. (1992) Effect of crack meandering on dynamic, ductile fracture. *J. Mech. Phys. Solids* **40,** 447–471.
Zhang, R., Zhang, X. and Hwang, K. C. (1983) Near-tip crack fields for plane strain Mode I steady state crack growth in linear hardening material with Bauschinger effect. *Proc. of ICF Int. Symp. on Fracture Mechanics*, pp. 283–290. Science Press, Beijing.
Zhang, X., Zhang, R. and Hwang, K. C. (1984) Near-tip fields for Mode I crack during steady growth in materials with mixed hardening (in Chinese). *Acta Mech. Sinica* **16,** 381–388.
Ziegler, H. (1959) A modification of Prager's hardening rule. *Quart. Appl. Math.* **17,** 55–65.

APPENDIX I

In the cylindrical coordinates (r, ϑ, z), the basis vectors $\mathbf{e}_r$, $\mathbf{e}_\vartheta$ and $\mathbf{e}_z$ are defined as

$$\mathbf{e}_r(\vartheta) = \mathbf{e}_1 \cos\vartheta + \mathbf{e}_2 \sin\vartheta, \quad \mathbf{e}_\vartheta(\vartheta) = -\mathbf{e}_1 \sin\vartheta + \mathbf{e}_2 \cos\vartheta, \quad \mathbf{e}_z = \mathbf{e}_3, \tag{A1.1}$$

and, therefore

$$\mathbf{e}_r'(\vartheta) = \frac{d}{d\vartheta}\mathbf{e}_r = \mathbf{e}_\vartheta, \quad \mathbf{e}_\vartheta'(\vartheta) = \frac{d}{d\vartheta}\mathbf{e}_\vartheta = -\mathbf{e}_r. \tag{A1.2}$$

When the asymptotic expansion (3.4_2) for the stress are introduced into the equilibrium (3.3) equations one obtains

$$\operatorname{div}[r^s \mathbf{T}(\vartheta)] = \mathbf{0}, \tag{A1.3}$$

which may be expanded to

$$r \operatorname{div} \mathbf{T}(\vartheta) + s\mathbf{T}(\vartheta)\mathbf{e}_r = \mathbf{0}. \tag{A1.4}$$

Finally, when the divergence operator is applied to the tensor $\mathbf{T}$ which is independent of the polar coordinate r, the equilibrium condition (A1.4) reduces to (3.7).

The components of the derivative with respect to ϑ of the stress tensor $\mathbf{T}$ in cylindrical coordinate may be derived by using relations (A1.2)

$$\begin{aligned}
(\mathbf{T}')_{rr} &= \mathbf{T}'\mathbf{e}_r \cdot \mathbf{e}_r = T_{rr,\vartheta} - 2T_{r\vartheta}, \\
(\mathbf{T}')_{r\vartheta} &= \mathbf{T}'\mathbf{e}_r \cdot \mathbf{e}_\vartheta = T_{r\vartheta,\vartheta} + T_{rr} - T_{\vartheta\vartheta}, \\
(\mathbf{T}')_{\vartheta\vartheta} &= \mathbf{T}'\mathbf{e}_\vartheta \cdot \mathbf{e}_\vartheta = T_{\vartheta\vartheta,\vartheta} + 2T_{r\vartheta}.
\end{aligned} \tag{A1.5}$$

Moreover, the components of the derivative with respect to ϑ of the velocity vector $\mathbf{w}$ may be found to be

$$\begin{aligned}
(\mathbf{w}')_r &= \mathbf{w}' \cdot \mathbf{e}_r = w_{r,\vartheta} - w_\vartheta, \\
(\mathbf{w}')_\vartheta &= \mathbf{w}' \cdot \mathbf{e}_\vartheta = w_{\vartheta,\vartheta} + w_r.
\end{aligned} \tag{A1.6}$$

APPENDIX II

The derivatives $\mathbf{T}'$ and $\mathbf{w}'$ at $\vartheta = 0$ are known from (4.9) and (4.11); therefore, Taylor series expansions of the stress tensor and velocity vector functions at $\vartheta = 0$ are possible

$$\mathbf{T}(\varepsilon) = \mathbf{T}(0) + \varepsilon\mathbf{T}'(0) + o(\varepsilon), \tag{A2.1}$$

$$\mathbf{w}(\varepsilon) = \mathbf{w}(0) + \varepsilon\mathbf{w}'(0) + o(\varepsilon). \tag{A2.2}$$

Moreover, Taylor expansions of the back stress and the flow stress may be performed at $\vartheta = 0$

$$\begin{aligned}
\mathbf{A}(\varepsilon) &= \mathbf{A}(0) + \varepsilon\mathbf{A}'(0) + o(\varepsilon), \\
T_F(\varepsilon) &= T_F(0) + \varepsilon T_F'(0) + o(\varepsilon),
\end{aligned} \tag{A2.3}$$

which are known, whence the values of $\mathbf{A}'$ and T_F' at $\vartheta = 0$ are derived.

In order to obtain these values, (3.6_1) is differentiated with respect to ϑ

$$\boldsymbol{\Sigma}' = (\mathbf{T}'' + s\mathbf{T}) \sin\vartheta - (1+s)\mathbf{T}' \cos\vartheta, \tag{A2.4}$$

and evaluated at $\vartheta = 0$ [assuming appropriate regularity conditions for angular function $\mathbf{T}$; see the discussion in Appendix B of Bose and Ponte Castañeda (1992)]

$$\boldsymbol{\Sigma}'(0) = -(1+s)\mathbf{T}'(0) = s(1+s)T_{rr}(0)(\mathbf{e}_2 \otimes \mathbf{e}_1 + \mathbf{e}_1 \otimes \mathbf{e}_2). \tag{A2.5}$$

Moreover, an evaluation of (3.12) at $\vartheta = 0$ results in

$$\mathbf{Q}(0) = \frac{3b}{2T_F(0)}\operatorname{dev}\mathbf{T}(0) + \frac{\phi}{2}\sinh\left(\frac{b\operatorname{tr}\mathbf{T}(0)}{2T_F(0)}\right)\mathbf{I}, \tag{A2.6}$$

so that $Q_{r\vartheta}(0) = 0$, and therefore, by (A2.5)

$$\mathbf{Q}(0)\cdot\mathbf{T}'(0) = 0, \quad \mathbf{Q}(0)\cdot\boldsymbol{\Sigma}'(0) = 0. \tag{A2.7}$$

Now, from (3.18), (4.3$_1$) and (4.7), we obtain $\rho(0) = -s/b$. Moreover, the derivative of (3.18) with respect to ϑ is

$$\rho' = \frac{\mathbf{Q}\cdot\boldsymbol{\Sigma}' + \mathbf{Q}'\cdot\boldsymbol{\Sigma}}{\mathbf{Q}\cdot\tilde{\mathbf{T}}} - \frac{\mathbf{Q}\cdot\tilde{\mathbf{T}}' + \mathbf{Q}'\cdot\tilde{\mathbf{T}}}{(\mathbf{Q}\cdot\tilde{\mathbf{T}})^2}\mathbf{Q}'\cdot\boldsymbol{\Sigma}, \tag{A2.8}$$

which gives, for $\vartheta = 0$

$$\rho'(0) = -\frac{s}{b^2}\frac{\mathbf{Q}(0)\cdot\mathbf{A}'(0)}{\mathbf{Q}(0)\cdot\mathbf{T}(0)}. \tag{A2.9}$$

The derivative of (3.16) with respect to ϑ, evaluated at $\vartheta = 0$, is

$$\mathbf{A}'(0)(1-s) = -(1-b)\frac{s}{b}\left[\frac{\mathbf{Q}(0)\cdot\mathbf{A}'(0)}{\mathbf{Q}(0)\cdot\mathbf{T}(0)}\mathbf{T}(0) + \mathbf{T}'(0) - \mathbf{A}'(0)\right], \tag{A2.10}$$

and the scalar product with $\mathbf{Q}(0)$ yields $\mathbf{Q}(0)\cdot\mathbf{A}'(0) = 0$, which introduced in (A2.9) gives $\rho'(0) = 0$. A substitution of this result into (A2.10) gives

$$\mathbf{A}'(0) = -s\frac{1-b}{b-s}\mathbf{T}'(0). \tag{A2.11}$$

The derivative of (3.17) with respect to ϑ, evaluated at $\vartheta = 0$, is

$$(1-s)T_F'(0) = b\rho(0)T_F'(0); \tag{A2.12}$$

therefore, considering that $\rho(0) = -s/b$, we obtain $T_F'(0) = 0$. When the expressions of $\mathbf{A}'(0)$ and $T_F'(0)$ are introduced into the series expansions (A2.3), the fields $\mathbf{A}$ and T_F can be evaluated at $\vartheta = \varepsilon$, as functions of the stress tensor $\mathbf{T}$ and its derivative $\mathbf{T}'$ at $\vartheta = 0$, given by (4.8) and (4.9)

$$\mathbf{A}(\varepsilon) = (1-b)\left[\mathbf{T}(0) - \varepsilon\frac{s}{b-s}\mathbf{T}'(0)\right] + o(\varepsilon), \tag{A2.13}$$

$$T_F(\varepsilon) = T_F(0) + o(\varepsilon), \tag{A2.14}$$

where $T_F(0)$ can be obtained by solving the system (4.15)–(4.16).

By using the relations (A1.1) in Appendix 1, the unit vectors of the cylindrical reference system assume the following expressions at $\vartheta = \varepsilon$

$$\begin{aligned}\mathbf{e}_r(\varepsilon) &= \mathbf{e}_r(0) + \varepsilon\mathbf{e}_\vartheta(0) + o(\varepsilon) = \mathbf{e}_1 + \varepsilon\mathbf{e}_2 + o(\varepsilon),\\ \mathbf{e}_\vartheta(\varepsilon) &= -\varepsilon\mathbf{e}_r(0) + \mathbf{e}_\vartheta(0) + o(\varepsilon) = -\varepsilon\mathbf{e}_1 + \mathbf{e}_2 + o(\varepsilon),\end{aligned} \tag{A2.15}$$

which are needed to obtain the components (4.19)–(4.21).